MINISTÉRIO DA CIÊNCIA E TECNOLOGIA
INSTITUTO NACIONAL DE PESQUISAS ESPACIAIS

INPE-8150-RPQ/717

CLIMATE CHARACTERISTICS IN AN ENSEMBLE SIMULATION USING THE CPTEC/COLA ATMOSPHERIC GLOBAL CIRCULATION MODEL

Iracema Fonseca de Albuquerque Cavalcanti
Prakki Satyamurty
José Antonio Marengo
Carlos Afonso Nobre
Igor Trosnikov
José Paulo Bonatti
Antonio Ocimar Manzi
Tatiana Tarasova
Cassiano D'Álmeida
Gilvan Sampaio
Christopher Cunninghan Castro
Marcos Sanches
Hélio Camargo
Luciano Ponzi Pezzi

INPE
São José dos Campos
2001

ACKNOWLEDGEMENTS

To Conselho Nacional de Desenvolvimento Científico e Tecnológico (CNPq) for the partial support during the research.

RESUMO

O Modelo de Circulação Global da Atmosfera (MCGA) CPTEC/COLA é integrado com nove condições iniciais, aplicando como condição de contorno forçante a Temperatura da Superfície do Mar mensal observada por 10 anos, para obtenção de uma climatologia e também para analisar a variabilidade interanual e o desempenho do modelo. Os resultados para cada estação do ano são comparados com dados observacionais, e precipitação mensal é analisada para várias regiões do globo. Uma avaliação do desempenho do modelo é apresentada através de uma análise de erros sistemáticos, correlação de anomalias, erro médio quadrático e reprodutibilidade. O modelo é capaz de simular as principais características do clima global e os resultados são consistentes com análises de outros MCGAs. A variabilidade sazonal é bem representada em todas as variáveis analisadas. A variabilidade espacial da precipitação também é bem simulada mas o modelo superestima os valores na parte sul da Zona de Convergência do Atlântico Sul, Zona de Convergência do Pacífico Sul e Zona de Convergência do Oceano Índico e subestima a parte norte destes sistemas. A precipitação na Amazônia, Indonésia e Oeste da África é subestimada quando comparada com os dados observacionais. As Altas subtropicais são bem detectadas nos campos de pressão e de ventos em baixos níveis mas os ventos alísios do Atlântico e do Pacífico são mais fracos que aqueles representados nos dados de reanálise. A localização e sazonalidade das correntes de jato subtropicais e as "storm tracks" são bem identificadas pelo modelo, embora mais intensas do que nos dados de reanálises e a Alta da Bolívia e Alta do Tibet são bem representadas. As ondas estacionárias do Hemisfério Norte e Sul são mais fracas nos resultados do modelo mas são bem simuladas em termos de número de onda. Os grandes erros que ocorrem na Cordilheira dos Andes indicam a deficiência na orografia do modelo. Análises de correlação e reprodutibilidade com respeito à precipitação indicam a região tropical como a mais previsível e com os mais altos valores de correlação entre os dados do modelo e os observados. Nos extratrópicos as correlações de anomalias são baixas mas as médias espaciais de precipitação em muitas dessas regiões simulam corretamente a variabilidade sazonal. Análises do balanço de energia indicam que os esquemas de parametrização de radiação e de nuvens precisam ser melhorados. É sugerido que mudanças nos esquemas de convecção e na resolução de orografia possam também melhorar o desempenho do modelo.

ABSTRACT

The Atmospheric Global Circulation Model CPTEC/COLA is integrated with nine initial conditions, applying as forcing boundary conditions the observed Sea Surface Temperature for 10 years to get the model climate on an ensemble mode and also to analyse the interannual variability and the performance of the model. Seasonal results are compared to observational data, and monthly precipitation is analyzed for several regions in the globe. Evaluation of the model's performance is presented through systematic errors, anomaly correlation, root mean square error (rms) and reproducibility. The model is able to simulate the main features of the global climate and the results are consistent with analyses of other AGCMs. Seasonal variability is well represented in all analyzed variables. Spatial variability of precipitation is well simulated, but the model overestimates the values in the southern portion of the South Atlantic Convergence Zone, South Pacific Convergence Zone and South Indian Convergence Zone and underestimates in the northern portion of these systems. The Amazon, Indonesia and Western Africa precipitation are underestimated when compared to the observed data. The subtropical highs are well detected in the pressure and low level wind fields but the Atlantic and Pacific trade winds are weaker than in the reanalysis data. The location and seasonality of subtropical jet streams and storm tracks are well depicted by the model, although more intense than in the reanalysis, and the high level anticyclones as the Bolivian and Tibetan Highs are well simulated. The stationary waves of the northern and southern hemispheres are weaker in the model, but are well represented in terms of wavenumber. Large errors over Andes Cordillera indicate the deficiency in the model orography. Correlation analyses and reproducibility with respect to precipitation indicate the tropical region as the most predictable and with highest correlation values, but the rms is also high in this region. In the extratropics, anomaly correlations are small, but the spatial averages of precipitation in many areas of these regions simulate correctly the seasonal variability and show low spread among members of the ensemble. Analysis of the energy budget indicates that the radiation and cloud scheme parametrizations need to be improved. It is suggested that changes in the convection scheme and in the orography resolution could also improve the model's performance.

CONTENT

LIST OF FIGURES

LIST OF TABLES

CHAPTER 1

INTRODUCTION

Global Circulation Models have been used in climate simulations for purposes of climate variability or climate change studies, seasonal prediction and also to verify their ability in describing the main features of the atmosphere. Results of long-run integrations are important to provide the model climatology, and to perform model validation. It is desirable that the model simulates well the current climate and the climate variability in order to give confidence in results of seasonal prediction, climate change and other model experiments. Simulation results have shown the ability of different models in representing observed characteristic features of the atmospheric circulation and precipitation. However, the intensity and geographical distribution of maximum values related to these features differ in each model. The continuous increase of the computer power enables increased model resolution, sophisticated parameterization schemes and large number of integrations, that lead to an improved simulation of the atmosphere. Improvements in parameterization schemes (Brankovic and Molteni 1997) and the increase of model resolution (Déqué et al. 1994) have reduced errors in model results. The chaotic behaviour of the atmosphere made the ensemble technique, imposing different initial conditions to the atmosphere, an useful way to improve model results (Murphy 1988). The ensemble method is used to indicate the range of possible climate outcomes for a given boundary forcing, typically SST (Mason et al. 1999).

Reviews of the ensemble climate modelling can be found in Brankovic and Palmer (1997), Li (1999), Rowell (1998), Wang and Zwiers (1999). The use of ensemble forecasts for seasonal prediction derives from the fact that such forecasts are essentially probabilistic. An ensemble forecast represents a collection of forecasts regarded as possible scenarios given the uncertainty associated with initial conditions and forecasting. Benefits and applications of this type of analysis include an efficient extraction of the model's forced

variability. Climate simulation is mainly a boundary-forced problem and model internal variability can be considered as noise. Even though the causes of model internal variability are not fully known, the use of ensemble means can partially overcome the problem of the model internal variability.

Rowell (1998) assessed potential seasonal predictability with an ensemble of multidecadal runs of the Hadley Center GCM, and showed that the highest predictability occurs over the tropical oceans, particularly the Pacific and Atlantic. Yang et al. (1998) used an ensemble of 8 members of a 10 year AMIP integrations to assess the potential predictability of the extratropical atmospheric seasonal variations. They found that potentially predictable regions during spring and winter were confined to the traditional Pacific North American (PNA) region while during summer and fall they were favored over the middle part of North America. Ward and Navarra (1997) performed an ensemble of three GCM integrations forced with observed SST through 1979/1988, and the significant reproducibility of climate anomalies in the central and western tropical Pacific among ensemble members indicated potential seasonal forecast skill.

Sensitivity analysis to changes in the ECMWF GCM formulation from 1990 to 1994 was performed by Brankovic and Molteni (1997). The development of more sophisticated physical parameterizations generated a better December-January-February (DJF) climatology than earlier versions and the zonal averaged precipitation was improved mainly in the tropics. The Inter Tropical Convergence Zone (ITCZ), South Pacific Convergence Zone (SPCZ) and South Atlantic Convergence Zone (SACZ) were better represented in the latest version, while in the extratropics the differences among the versions were relatively small. As in the ECMWF GCM, the Hadley Centre Coupled Ocean-Atmosphere GCM (HADCM2) also shows underestimation of the zonally averaged precipitation in the Southern Hemisphere DJF storm track region (Johns et al. 1997). However, in June-July-August (JJA) the model values are larger than the climatological values of Legates and Willmott (1990a), but

similar to observational data of Jaeger (1976). The model results in this region are more similar to Xie and Arkin (1997) data in both seasons. Applying a band-pass filter to isolate synoptic scale variability, Johns et al. (1997) showed good agreement between the model and observed areas of storm tracks in both hemispheres. HADCM2 also reproduces quite well the positioning and shape of the main sea surface pressure centers, although some centers have different intensities when compared to observational data. There were significant errors in the positioning and strength of the main jets in both hemispheres associated with systematic temperature bias. The main errors related to the atmospheric temperature showed a cold bias in the troposphere and a warm bias in the stratosphere.

A detailed performance analysis of the NCAR Community Climate Model (version CCM3) was documented in Hurrel et al. (1998), Kiehl et al. (1998) and Hack et al. (1998). Aspects of the dynamical simulation were discussed in Hurrel et al. (1998), the hydrologic and thermodynamic climatology presented in Hack et al. (1998) and the energy budget in Kiehl et al. (1998). The model represented well the basic observed patterns of several variables, although some features were displaced from the observed location and had different intensities. Compared to Xie and Arkin precipitation, the model simulates well the South Atlantic Convergence Zone and the South Pacific Convergence Zone in DJF, as well as the ITCZ over the Pacific Ocean. However, the Atlantic ITCZ was not well reproduced by the model. The zonal averaged precipitation had larger values than Xie and Arkin observational data in the storm track regions of both hemispheres, but comparable to the data of Legates and Willmott in DJF, mainly in the Southern Hemisphere storm track region. The model captured the major troughs and ridges of the Northern Hemisphere and some characteristics of the wavenumber one in the Southern Hemisphere. The middle-latitude westerlies were too strong between 40^0 and 50^0 of both hemispheres during both winter and summer. The trade winds were also stronger than observations, consistent with the enhanced subtropical high-pressure centers in the model (Hurrel et al. 1998).

The subtropical high-pressure centers were also enhanced in the climatology of the Canadian Climate Centre GCM, but the pressure was lower than observations in the high northern latitudes (Mc Farlaine et al. 1992). The simulated zonal averaged precipitation had larger values in the Northern Hemisphere storm track and smaller values in the Southern Hemisphere storm track than Jaeger (1976) observational data in both seasons. The tropical zonal mean precipitation was well simulated, mainly in DJF. However, in this season, precipitation over South America was poorly simulated. The model underestimated rainfall over South America and overestimated over the Indian Ocean.

Several GCMs were used in the Atmospheric Model Intercomparison Project (AMIP) to simulate the present climate and to analyze the results related to different parameterizations and resolutions, but subjected to the same initial condition and SST boundary condition (Gates 1992). Global hydrological processes were discussed in Lau et al. (1996) comparing 29 model results. The global mean surface air temperature and precipitation over land were shown in a scatterplot diagram, which indicated how far were the model results from the observations. Although there was large variability among models, the model ensemble mean was very close to the observations. An important result of Lau et al. (1996) is the deficiency of all models in simulating the light rain rates (0-1 mm/day). This result was a reflection of the poorly represented low-level stratocumulus and shallow convection. The zonal mean precipitation was better represented in JJA than in DJF in the ITCZ region. However, the latitudinal variability related to a maximum in the tropics, secondary maxima in both hemispheres associated to the storm tracks and the minima in subtropical regions, were simulated by the majority of models in both seasons. The ensemble spatial distribution of global precipitation represented the main rainfall features associated with ITCZ, SPCZ, Asia summer monsoon and extratropical storm tracks. However, the model ensemble overestimated the rain in the tropics and underestimated in the extratropics. Other results of AMIP were discussed by Gates et al. (1999) who showed the model's ensemble errors of

several variables. The largest relative errors of the ensemble mean were found in the cloudiness and 200 hPa temperature and the smallest errors were identified in the surface air temperature. The need of further work to reduce the errors of the atmospheric GCMs was outlined by Gates et al. (1999) following the analyses of AMIP results.

In this study results from a climate simulation obtained running the CPTEC/COLA AGCM for 10 years are discussed and compared to observational data. The model is integrated with nine initial conditions to provide an ensemble mean. Results are analysed seasonally and the monthly variation of individual members is investigated in several areas of the globe. A description of the model and observed data sets for validation is presented in section 2, and the model results compared to observations are shown in section 3. Skill scores and statistical analyses are discussed in section 4. Discussions and conclusion are summarized in section 5.

CHAPTER 2

MODEL DESCRIPTION, EXPERIMENT DESIGN AND OBSERVATIONAL DATA SET

2.1 MODEL DESCRIPTION

CPTEC/COLA GCM is a modified version of the spectral COLA GCM, which was derived from the National Centers for Environmental Prediction (NCEP) GCM. A land surface module (Simple Biosphere Model, SIB) that considers the vegetation influence in a sophisticated manner (Xue et al. 1991) was introduced by COLA. Other modifications by COLA were related to radiation and cloud-radiation interactions and treatment of vertical diffusion. These modifications are documented in Sato et al. (1989) and Hou (1990). The COLA AGCM has now two options for convective precipitation, the Kuo scheme and the Relaxed Arakawa-Schubert scheme (Moorthi and Suarez 1992).

The dynamical and physical processes in the COLA model are described in Kinter et al. (1997). The CPTEC/COLA dynamical processes and physical parameterizations are the same as those of COLA model, with Kuo scheme for deep convection (Kuo, 1974); shallow convection parameterized following Tiedke (1983); Mellor and Yamada closure scheme applied for the vertical diffusion in the planetary boundary layer (Mellor and Yamada 1982) and biharmonic type diffusion for the horizontal diffusion necessary to control small scale noise. The shortwave radiation is that of Lacis and Hansen (1974) modified by Davies (1982) and the longwave formulation was developed by Hashvardhan et al. (1987). Cloud radiation interaction considers predicted clouds using a hybrid scheme of Hou (1990) and NCAR CCM2 scheme (Kihel et al. 1994). The Hou scheme is based on cloud prediction of Slingo (1987).

The lower boundary conditions are surface temperature over land and oceans,

sea ice, soil moisture, surface albedo and snow depth. Only Sea Surface Temperatures (SST) are monthly observed data. Sea ice is considered in grid points with SST below -2^0C. The other lower boundary conditions are introduced as initial conditions using the climatological surface temperature, soil humidity and albedo which are adjusted during the integration. Surface temperature and soil moisture climatological data are taken from Willmott et al. (1985). Climatological albedo is based on Posey and Clapp (1954). The snow depth is also applied as an initial condition based on the time interpolated surface albedo on the initial date of the model run (Kinter et al. 1997). Ozone concentration is interpolated from a climatological table which gives values at each 5^0 latitude for each sigma level and has different values for each season. Carbon dioxide has a constant value of 345 ppm. The upper boundary condition is kinematic and states that the vertical velocity at the top of the atmosphere must be zero, to satisfy mass conservation (Kinter et al. 1997).

The main changes introduced by CPTEC in the COLA GCM are related to the kind of truncation, dissipation process, computer performance, post-processing scheme and increase of the vertical levels. The truncation, which was rhomboidal is changed to triangular. In triangular truncation the horizontal resolution in the zonal and meridional directions is nearly the same. In rhomboidal truncation, the latitudinal resolution is the same for every zonal wavenumber. At high resolution, the triangular truncation appears to be superior (Holton 1992). All model numerical codes are rewritten considering triangular truncation. New compilation options are introduced to adapt the model to NEC-SX3/SX4 supercomputer. There are recodifications to improve the vectorization process, the performance, and to include the parallelization process. In order to prevent computational instability that arises from strong winds, an additional dissipation (Newtonian dissipation) is introduced in the wind tendency in the troposphere and low and high stratospheres.

Another modification in the program is the inclusion of routines to transform pressure coordinates variables into sigma coordinates and to transform zonal

and meridional wind components, temperature and relative humidity variables in divergence, vorticity, virtual temperature and specific humidity. The post-processing is written to accept the triangular truncation and to improve its performance. A more suitable extrapolation in regions of mountains is applied, mainly for temperature and humidity. Streamfunction and velocity potential fields are adjusted to wind field in pressure coordinates. The latest version of the model is prepared to run in a flexible, versatile and friendly form.

2.2 SIMULATION DESIGN

The model resolution in this simulation is T62L28, with triangular truncation of 62 waves in the horizontal coordinate and 28 levels in the vertical sigma coordinate (21 in the troposphere and 7 in the stratosphere). The climate simulation is performed in an ensemble mode, integrating the model with 9 different initial conditions derived from 9 consecutive days of ECMWF daily analyses, from 11 to 19 September 1981. Spectral data of temperature, zonal and meridional wind components and relative humidity are transformed to spectral virtual temperature, divergence, vorticity, specific humidity and logarithm of pressure, which are the initial conditions for each day. Surface pressure is calculated from the geopotential, temperature and topography. Monthly observed Sea Surface Temperature (SST) from Climate Prediction Center /NCEP monthly Optimum Interpolation SST dataset (Reynolds and Smith 1994) are applied as forcing boundary conditions, from 1981 to 1991. The spinup time for adjustments of the climate conditions of soil moisture and albedo is two and a half months.

The results are analyzed from December 1981 to November 1991, considering the seasonal averages for each variable under consideration. Ensemble means are taken to compare the model results to observational datasets. The analyzed variables are precipitation, sea surface pressure, wind field at 850 and 200 hPa, geopotential height at 200 hPa and outgoing longwave radiation (OLR).

Precipitation fields are shown for all seasons while the other variables are shown for DJF and JJA. Monthly mean precipitation over land, in the Northern and Southern Hemispheres as well as in other areas of the globe are also displayed to show the behaviour of different members. Other analyzed fields are zonal mean vertical cross sections of zonal and meridional wind components, air temperature and mean meridional cells. Vertical cross-sections of geopotential zonal anomalies at subtropical and high latitudes of Southern and Northern Hemispheres are displayed to show the vertical structure of the stationary waves. Global energy fluxes, albedo and cloud fraction are calculated to show the model energy budget.

2.3 OBSERVATIONAL DATA SETS

Global and regional precipitation rainfall fields are derived from the Climate Prediction Center Merged Analysis Precipitation (CMAP) data (Xie and Arkin 1997) available from 1979 to 1996. The CMAP data set uses several estimates of precipitation as measured by satellite over land and oceans, as well as the raingauge data over land. In this study, only the period of the model integration (1982-1991) was taken to compare the seasonal climatology. Other data sets include the corrected gauge-derived rainfall climatology of Legates and Willmott (1990). This data set includes shipboard raingauge corrected data interpolated on a grid of 0.5 latitude x 0.5 longitude. In this case, the climatology is considered for the period of 1920-1980, with greater weight given to the more recent years.

NCEP/NCAR reanalysis (Kalnay et al. 1996) are used to validate wind fields, sea surface pressure, temperature and geopotential height. OLR is taken from NOAA data set obtained by satellite measurements (Liebman and Smith 1996).

CHAPTER 3

MODEL CLIMATOLOGY AND OBSERVATIONS

In this section zonal means of precipitation and wind are analyzed in DJF and JJA and the spatial distributions of precipitation are shown for all seasons. Wind field, pressure, OLR and geopotential height zonal anomaly fields are displayed for DJF and JJA. The model results are compared to the observational fields.

3.1 ZONAL MEANS

A useful overview of the accuracy of the ensemble model climatology is given by zonally averaged statistics. The results for December-January February (DJF) and June-July-August (JJA) extremes of the annual cycle are shown in Fig. 3.1a,b. The zonal averaged precipitation is better simulated in JJA in the Northern Hemisphere (NH), comparing very well with both Legates and Willmott (1990) and CMAP. We note that the model tends to overestimate observed precipitation in the NH during northern winter and in the Southern Hemisphere (SH) during austral summer (Fig. 3.1a), when compared to CMAP climatology, while when compared to Legates and Willmott the model underestimates rainfall between 60^0-90^0S.

In JJA precipitation is very well simulated in the tropics with its peak north of the equator. The model, in general, significantly overestimates the precipitation in comparison with the observed data sets, except in polar latitudes beyond 75^0, subtropics (around 35^0S, 40^0N) and over the equator. The model simulation is closer to Legates and Willmott data set in the NH and to CMAP in the SH. Pronounced overestimation of midlatitude precipitation in SH indicates that the model produces more intense and/or more frequent cyclogenesis in the storm track region. The position of the simulated subtropical precipitation minima, associated with the subtropical

agreement with the Legates and Willmott data set.

In DJF (Fig. 3.1a) there are more discrepancies between the model and the observational data sets, but the model can capture important features like the double maximum in the tropical region and the storm track region of both hemispheres. The latitude of the minima associated with the southern subtropical highs and at high latitudes agrees with both observational data sets, the values being closer to CMAP data set. The maximum value at 60^0S of Legates and Willmott is too high in DJF, when compared to CMAP and Jaeger (1976) data set analyzed by Johns et al. (1997).

Model precipitation in the tropical region reaches up to 6 mm/day near 5^0 N, which is ~1.6 mm.day^{-1} larger than the CMAP data set, and almost identical to Legates and Willmot estimates. For the Southern Hemisphere, the model does not simulate the observed maximum near 10^0 S, but rather has a broad peak around 15^0 S. The subtropical minima are well simulated in the winter hemisphere. During both seasons, modeled precipitation rates are higher than the observed estimates from CMAP over the midlatitude storm tracks, although the Legates and Willmott show rainfall rates of ~2 mm.day^{-1} higher in the summer hemisphere. The large rainfall rates in the equatorial latitudes are associated with strong convection in the ITCZ, which migrates north and south in different seasons. The variability and intensity of the ITCZ (rainfall and convection in equatorial latitudes) is well depicted by the model.

Other models, like CCM3 (Hurrel et al. 1998), HADACM3 (Johns et al. 1997), ECMWF (Brankovic and Molteni 1997), also show smaller values than Legates and Willmott in the secondary maximum related to DJF Southern Hemisphere storm track. As pointed out by Brankovic and Molteni (1997), the observational data of Legates and Willmot can have some errors at high latitudes in the Southern Hemisphere, related to lack of information. The maximum tropical precipitation of CPTEC/COLA GCM is closer to the values of Legates and

Willmot in JJA (Fig. 3.1b) than the results of HADACM3 (Johns et al. 1997) and NCAR CCM3 (Hurrel et al 1998). These models have lower horizontal and vertical resolutions than CPTEC/COLA GCM, and different parametrizations.

The zonal mean sea level pressure SLP (Fig. 3.1c,d) represents well the equatorial trough, the subtropical highs and the low pressure at high latitudes. The model estimates higher SLP in the tropics and subtropics, irrespective of the season and hemisphere. There are larger differences in the Northern Hemisphere polar region than in other latitudes, and the subtropical highs are overestimated by the model. The latitudes of the subtropical highs are consistent with the minima in precipitation only in the summer hemisphere. In the winter hemisphere the maximum sea level pressure is located polewards of the minimum precipitation. The low pressure around Antarctica is well simulated in both seasons. The model tends to overestimate the SLP by about 1 hPa in equatorial latitudes, while the difference can reach up to 4 hPa in mid latitudes. However, at high northern latitudes in DJF (Fig. 3.1c) and in JJA (Fig. 1d) the disagreement can reach up to 5 hPa.

Another example of model validation is given by the 200 hPa zonally averaged zonal winds, shown in Figs. 3.1e,f for DJF and JJA, respectively. A reasonably good simulation of the overall circulation structure and the seasonal shifts of the maxima and minima are noticed, which are reflections of the model success in simulating the mean meridional tropospheric temperature gradients. In JJA, the model reproduces very well the intensity of the westerlies in the Northern Hemisphere and shows close values in the Southern Hemisphere and in the tropical easterlies region. In DJF the model overestimates the NCEP reanalysis values in the jet region of both hemispheres, with larger differences in the Southern Hemisphere, and in the region of tropical easterlies. The overestimated intensities of the westerly jets are smaller in Northern Hemisphere than in Southern Hemisphere, and larger in southern summer (10 ms^{-1}) than in southern winter (3 ms^{-1}).

The overestimation of precipitation in SH discussed above is consistent with stronger jet in the mid latitudes of this hemisphere. The meridional shear of the zonal wind is stronger in the model simulation in DJF which may have repercussions on the barotropic development of synoptic disturbances. The low level modeled zonal wind fields (not shown) for DJF and JJA agree remarkably well with the observed fields, regarding the position and intensity of the tropical easterlies and the extratropical westerlies.

a)

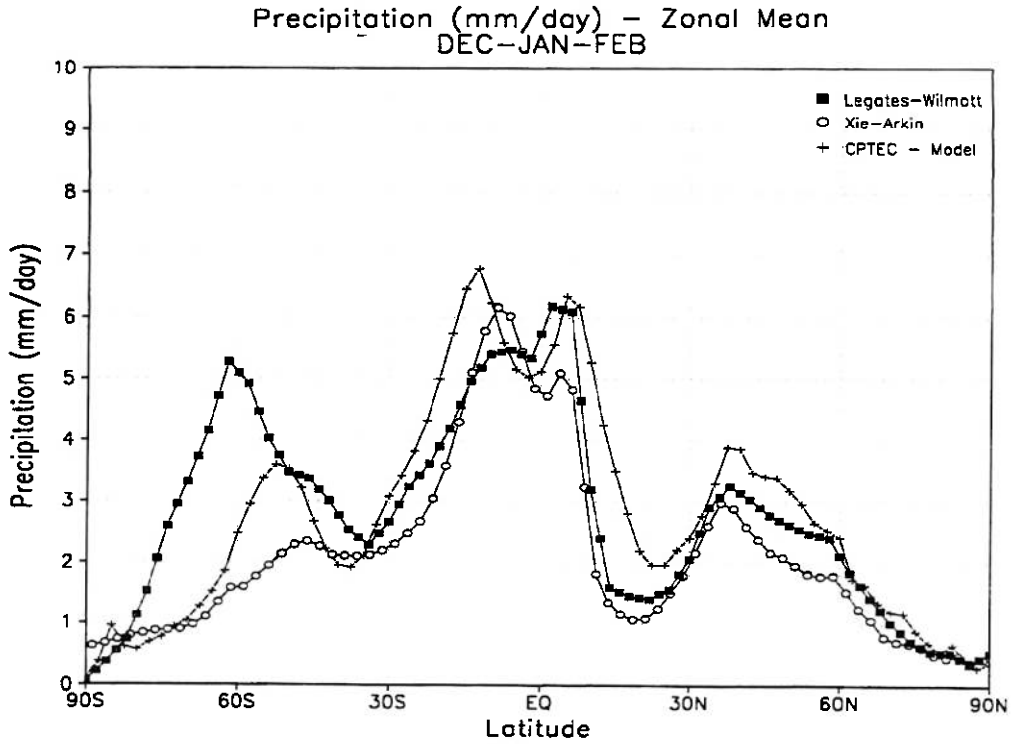

b)

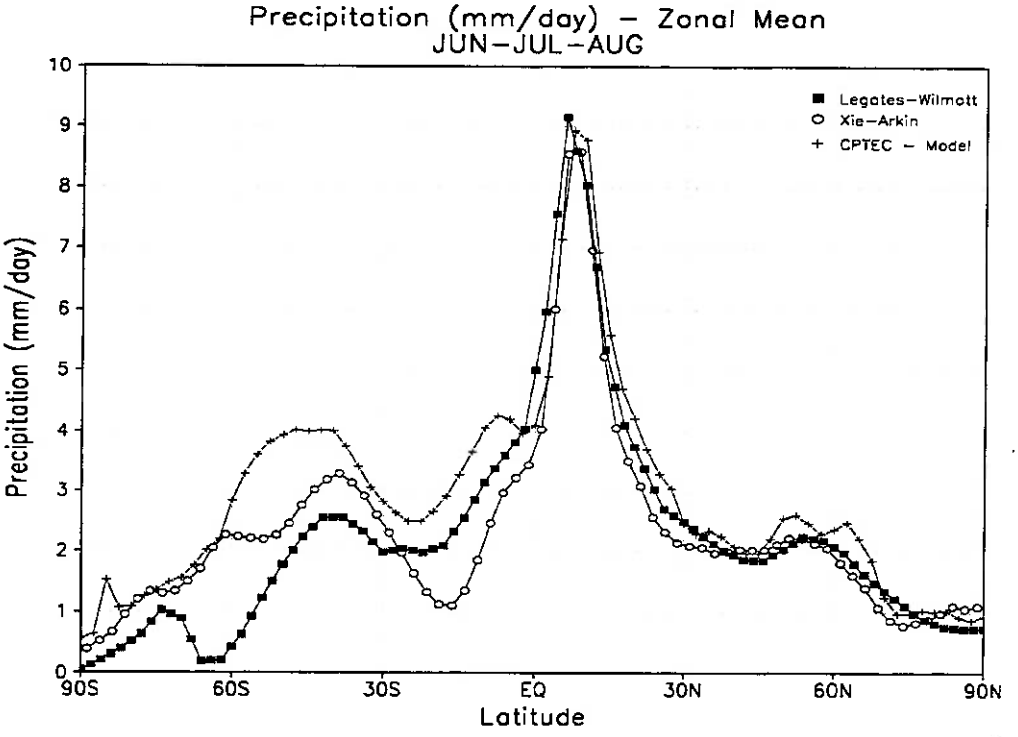

Fig. 3.1 – Zonal mean precipitation (a) DJF, (b) JJA, pressure (c) DJF), (d) JJA, zonal wind at 200 hPa (e) DJF, (f) JJA for the ensemble mean and observed data. Observed precipitation from Legates and Wilmot (1990) and CMAP (Xie and Arkin 1997). Observed pressure and wind fields are taken from NCEP/NCAR reanalysis data.

(continue)

c)

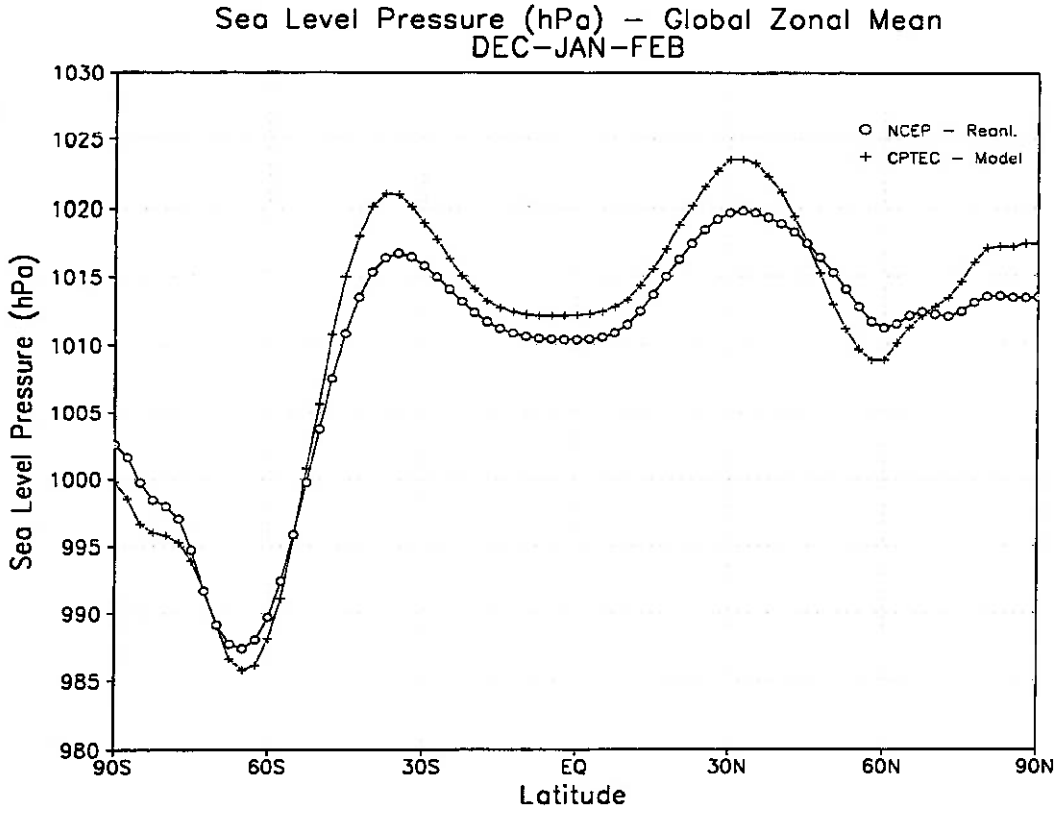

d)

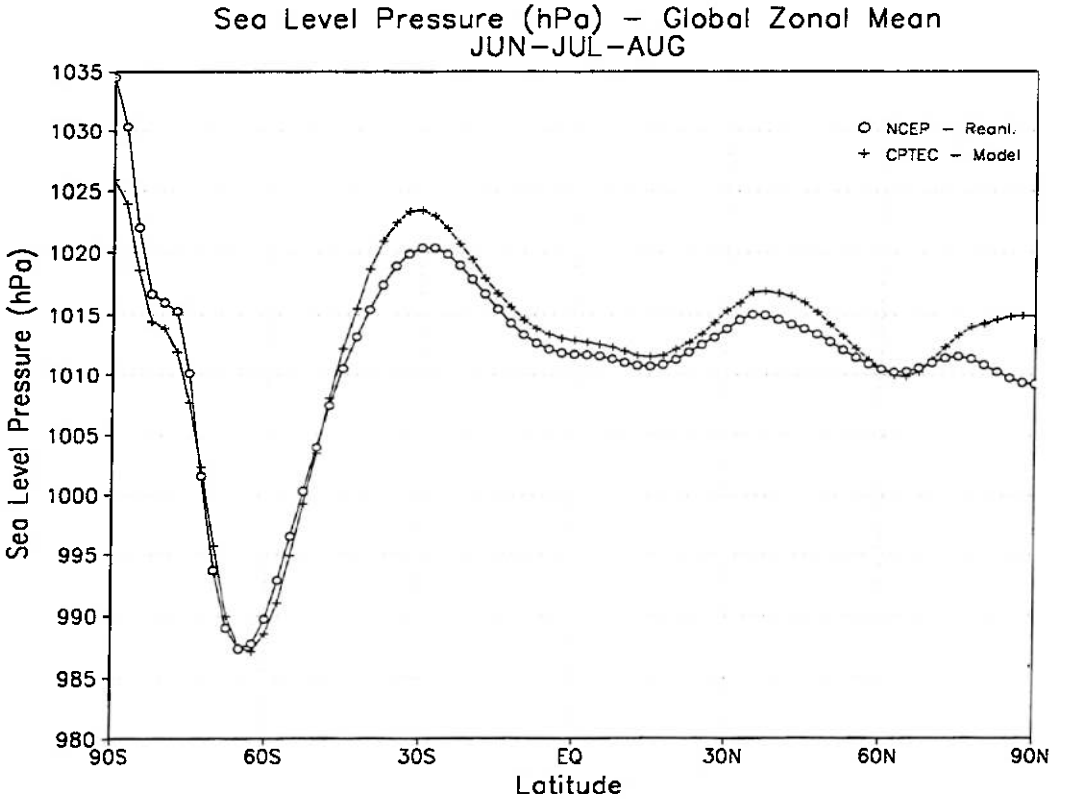

Fig. 3.1- (continue)

e)

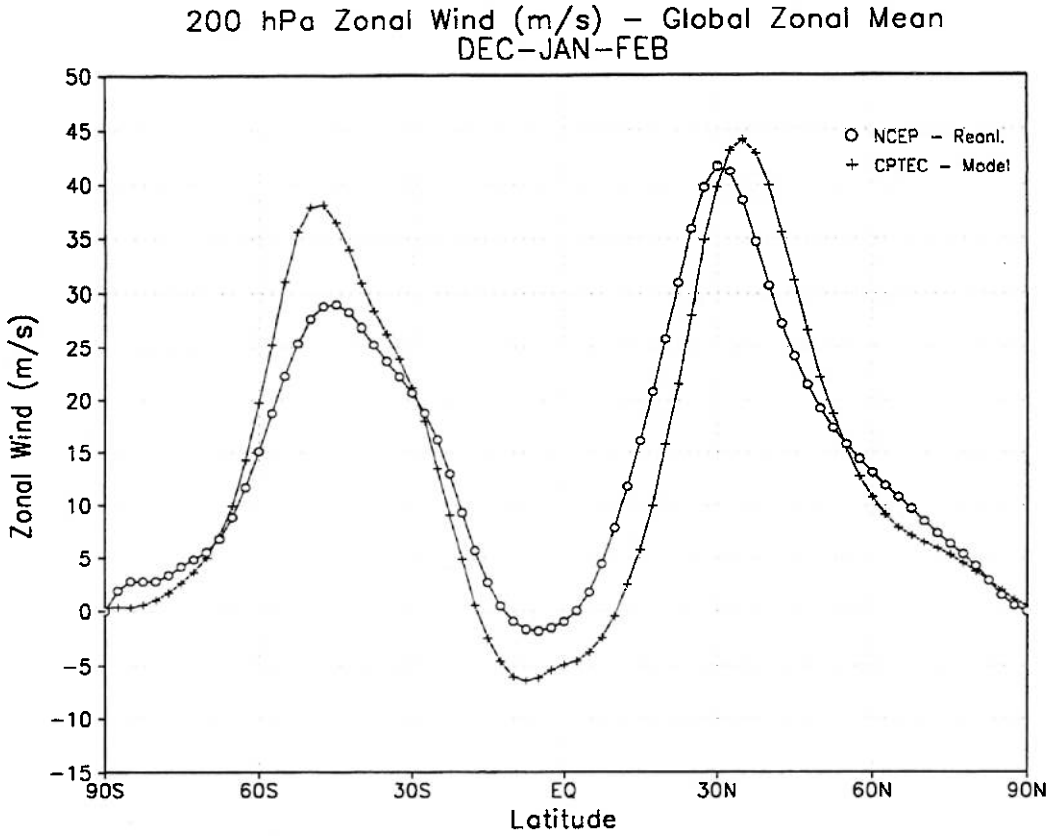
200 hPa Zonal Wind (m/s) – Global Zonal Mean
DEC–JAN–FEB
O NCEP – Reanl.
+ CPTEC – Model
Zonal Wind (m/s)
50
45
40
35
30
25
20
15
10
5
0
−5
−10
−15
90S
60S
30S
EQ
30N
60N
90N
Latitude

f)

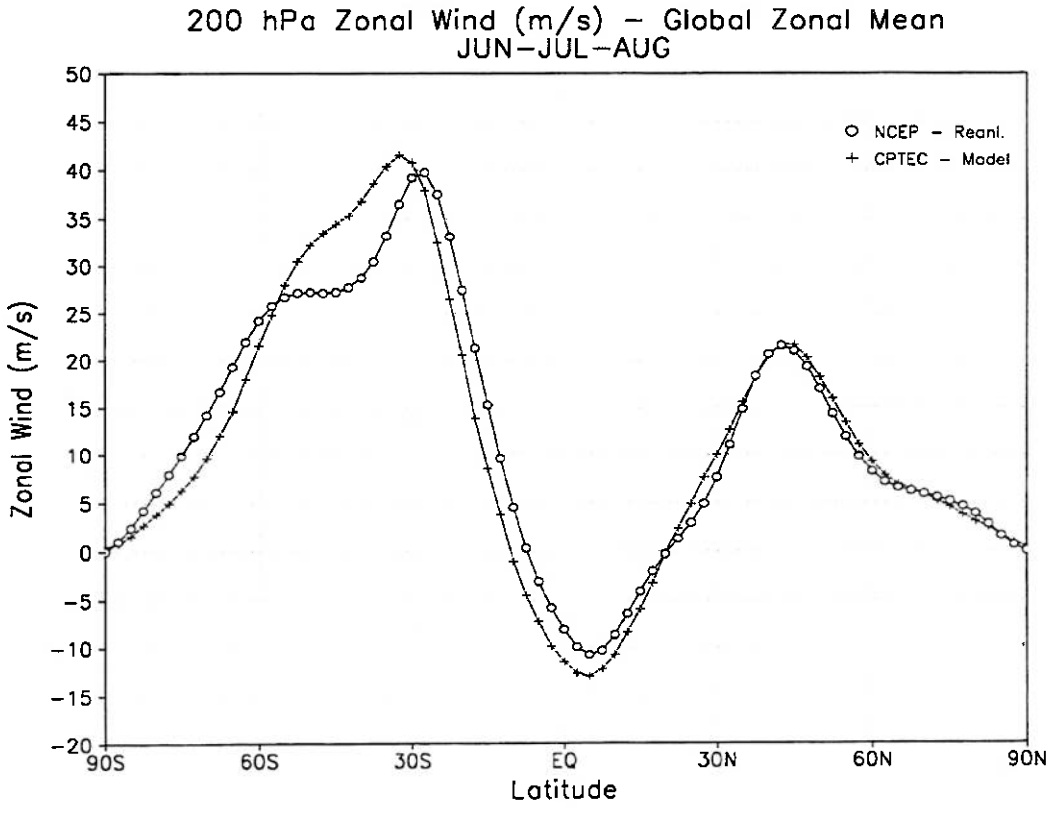
200 hPa Zonal Wind (m/s) – Global Zonal Mean
JUN–JUL–AUG
O NCEP – Reanl.
+ CPTEC – Model
Zonal Wind (m/s)
50
45
40
35
30
25
20
15
10
5
0
−5
−10
−15
−20
90S
60S
30S
EQ
30N
60N
90N
Latitude

Fig.3.1-

(end)

3.2 MAIN CLIMATOLOGICAL FEATURES SIMULATED BY THE MODEL

The seasonal variability of precipitation is well represented in the simulation, as shown in Fig. 3.2a-l. These figures show the model, CMAP and the systematic errors of seasonal precipitation. The displacement of the Atlantic ITCZ, southwards in DJF and MAM, and northwards in JJA and SON, is well depicted by the model. The model overestimates the values in the Atlantic ITCZ, and except in DJF, the differences tend to be large close to South America and Africa coasts. The Pacific ITCZ is also overestimated, with larger differences over East Pacific. Over West Pacific the errors are related to ITCZ shifting northwards. Precipitation associated with the SPCZ and SACZ is also well simulated, the SPCZ occurring during the whole year, and the SACZ in DJF.

These features are also identified in OLR fields, (Fig.3.3a-f) in which the ITCZ activity and the latitudinal displacement are well simulated but the Pacific ITCZ activity is overestimated, consistent with the precipitation field. The activities of the SPCZ and SACZ are reasonably reproduced by the model while areas without convective activity, such as the eastern side of the oceans, and Sahara, have higher values of OLR in the model results than in the observed data. As the precipitation rate is well simulated in the regions of the subtropical highs, the radiation processes present some deficiencies likely related to the influence of the low level clouds which are poorly represented by the model.

The Subtropical Pacific and Atlantic Highs are reproduced in both hemispheres, although in the SH the intensity is higher in DJF in the model results than in the NCEP/NCAR reanalysis data (Fig. 3.4a,b,c). In general, all the subtropical high pressure cells are stronger in the CPTEC/COLA model simulation than in the NCEP/NCAR reanalysis. Low pressure over South America, South Africa and Indonesia region are noticed in DJF (austral summer) and in the northeast Asia in JJA (boreal summer), associated with surface heating. Low pressure is replaced by high pressure in the winter hemisphere in these regions. These

features are seen in both model results and reanalysis data. The highest and persistent errors in the SH surface pressure are found in Australia/New Zealand region. In the NH the largest errors occur over Greenland and Europe in DJF (Fig. 3.4c). As these regions in both hemispheres are regions of blocking situations, the model seems to enhance blocking in the North Atlantic and to weaken blocking in the Australia region. The anticyclonic circulations associated with the subtropical highs are shown in the lower tropospheric flow at 850 hPa (Fig. 3.5a,b,d,e).

3.2.1 - Features over South America and adjacent oceans

Seasonal variability is well simulated over South America. However, in DJF there is intense precipitation associated with an enhanced SACZ, and the Amazonia precipitation is underestimated by the model (Fig. 3.2 a, b). The model overestimates the precipitation in the southeast part of the SACZ, but underestimates the values in the northwest part of this system (Fig. 3.2c). The underestimation of convective activity over Amazonia is also seen in the OLR fields (Fig. 3.3a-c). In the observational data there is strong activity in DJF, extending to the southeast, characterizing the SACZ, while in the model the activity is concentrated in the southern portion of this system.

The excessive precipitation in the eastern Pacific ITCZ and in the southern part of SACZ may contribute to the deficiency of model rainfall over Amazonia. Other models also show deficiencies in representing the precipitation over West Amazonia, like ECMWF (Brankovic and Molteni 1997), NCAR CCM3 (Hurel et al. 1998), GFDL (Stern and Miyakoda 1995). However, HADACM3 (Johns et al. 1997), which is a coupled atmosphere-ocean model, gives DJF precipitation over Amazonia closer to observations than the other models, including CPTEC/COLA. Improvements of the precipitation rates over Amazon rainforest were shown in model experiments of Marengo et al. (1993), changing the ground hydrology in the Goddard Institute for Space Studies (GISS) GCM.

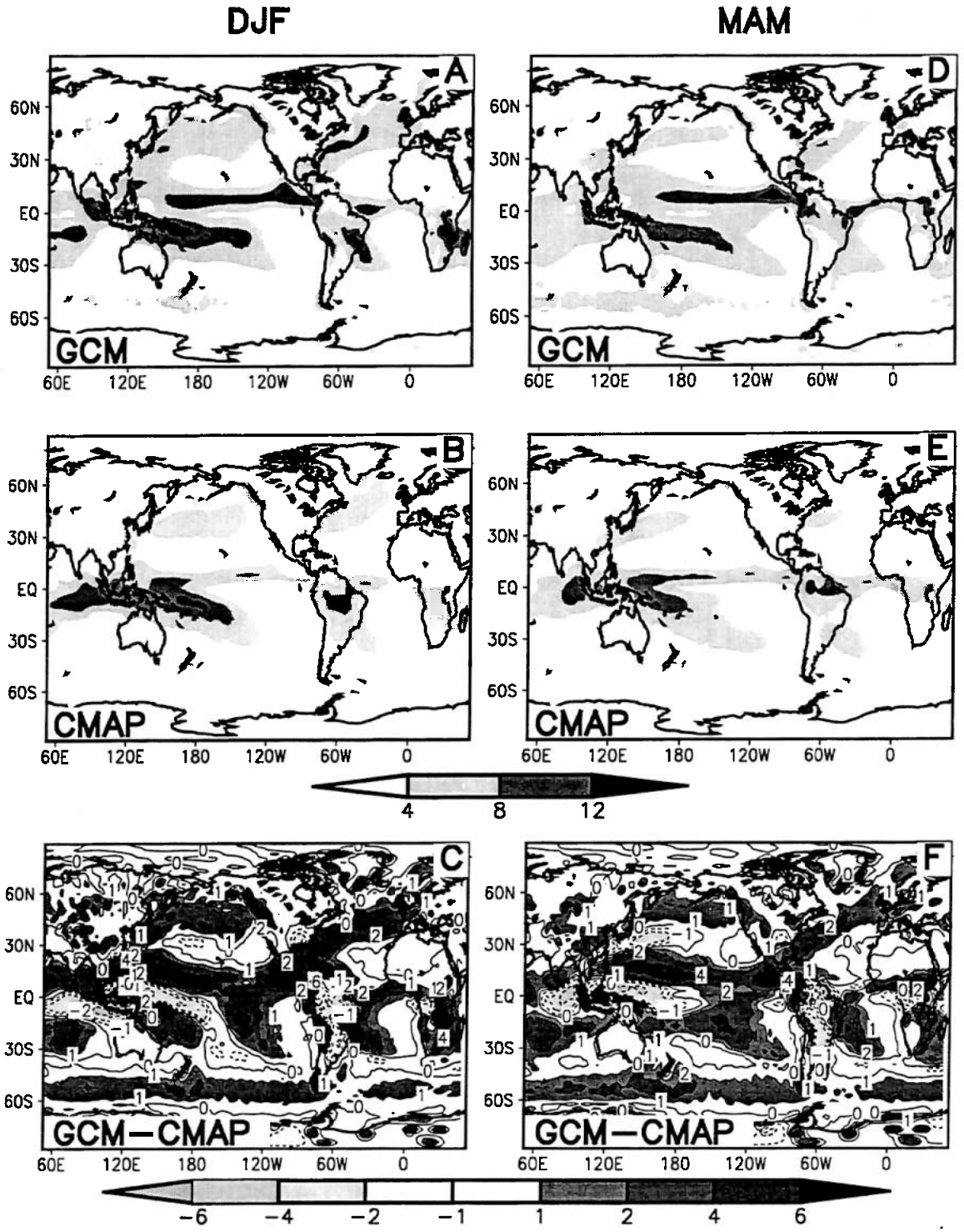

Fig. 3.2 – Climatological precipitation (a) DJF CPTEC/COLA AGCM, (b) DJF CMAP, d) MAM CPTEC/COLA AGCM, (e) MAM CMAP, (g) JJA CPTEC/COLA AGCM, (h) JJA CMAP, (j) SON CPTEC/COLA AGCM, (k) SON CMAP, (c), (f), (i), (l) are the differences between model and observation (mm.day $^{-1}$).

(continue)

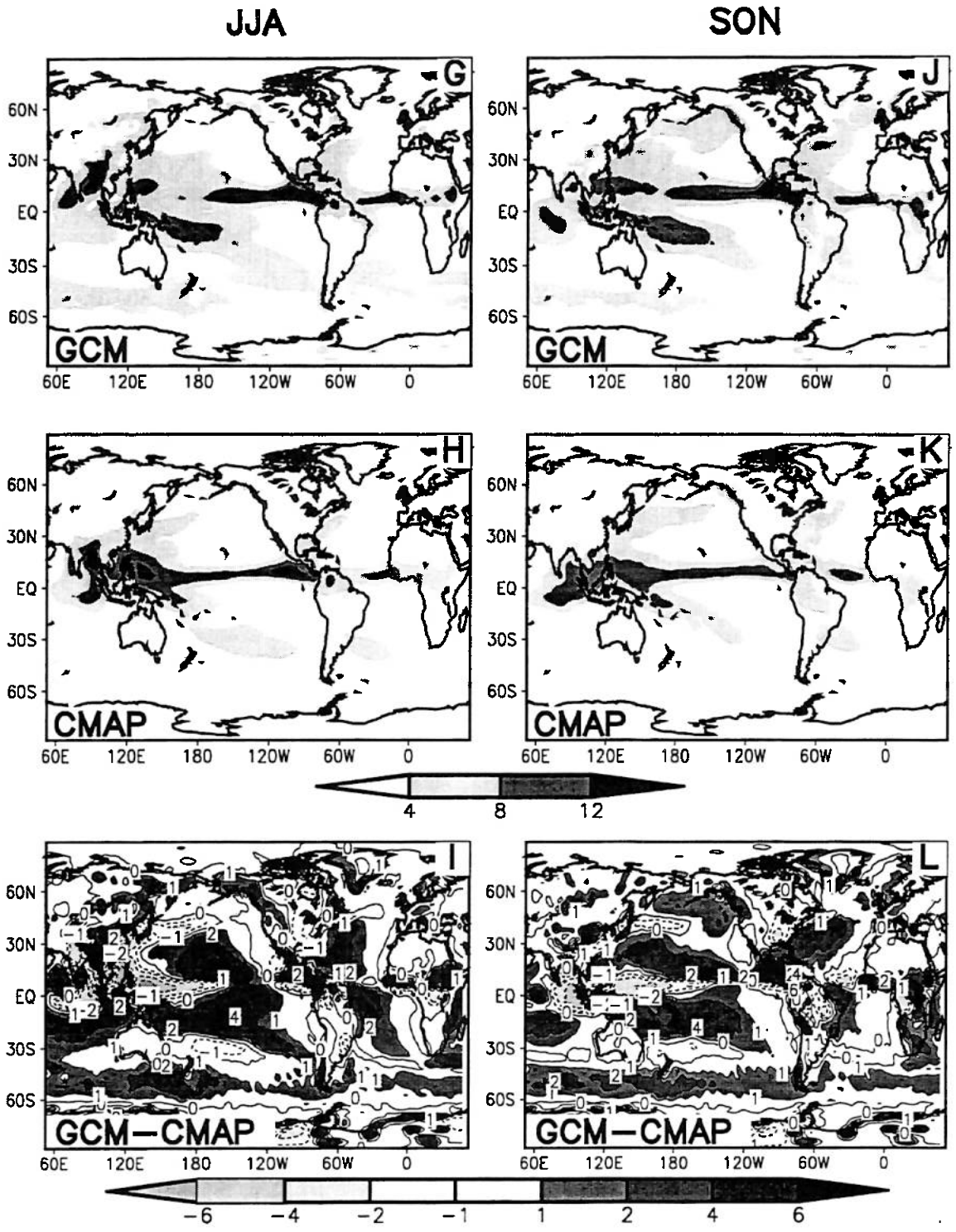
JJA
SON
G
J
H
K
I
L
GCM
CMAP
GCM−CMAP
60N
30N
EQ
30S
60S
60E
120E
180
120W
60W
0
4
8
12
−6
−4
−2
−1
1
2
4
6

Fig.3.2-

(end)

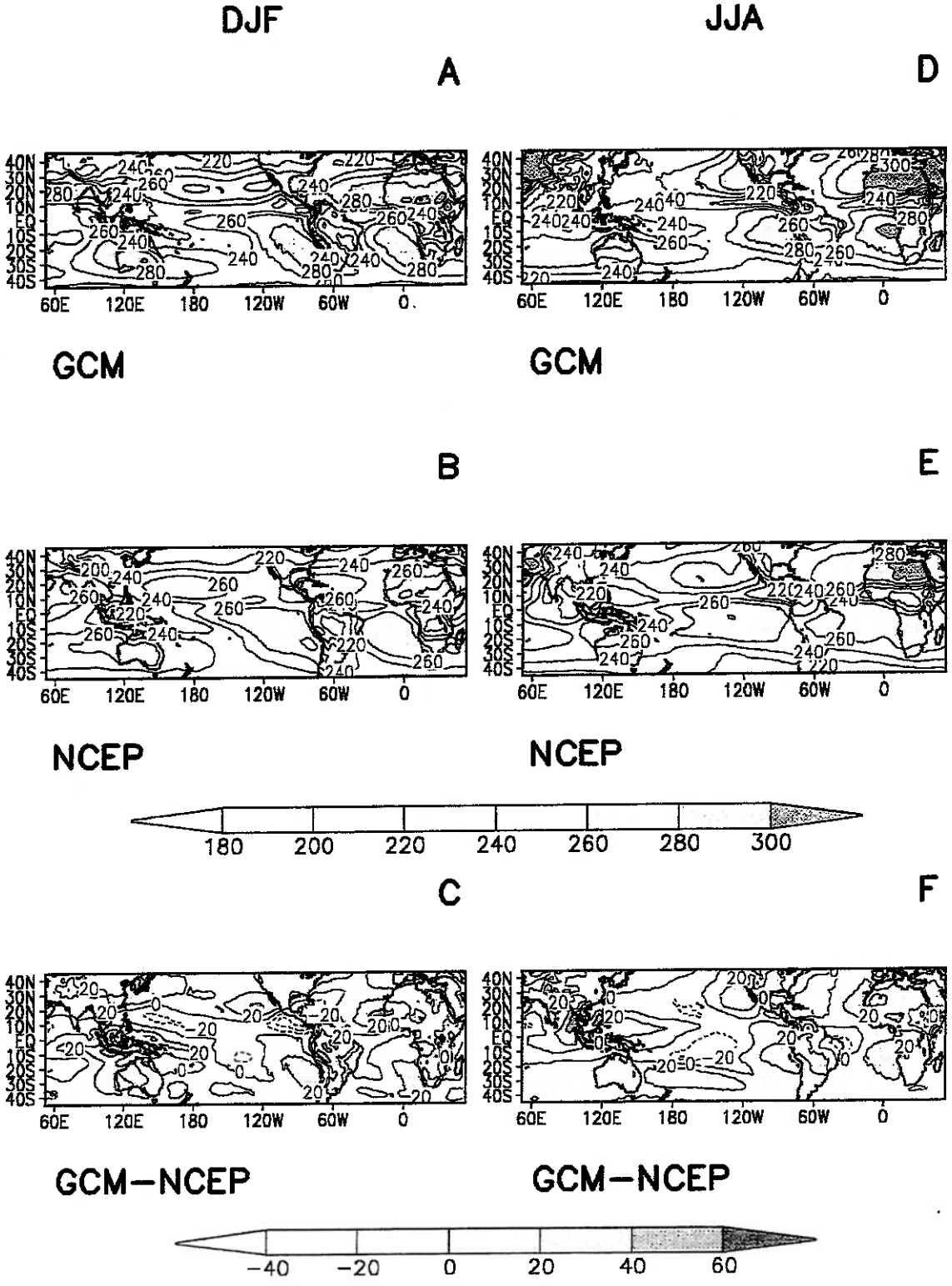

Fig. 3.3 – Climatological OLR (a) DJF CPTEC/COLA AGCM, (b) DJF NOAA data set, (d) JJA CPTEC/COLA, (e) JJA NOAA data set, (c), (f) are the differences between the model and observations ($W.m^{-2}$).

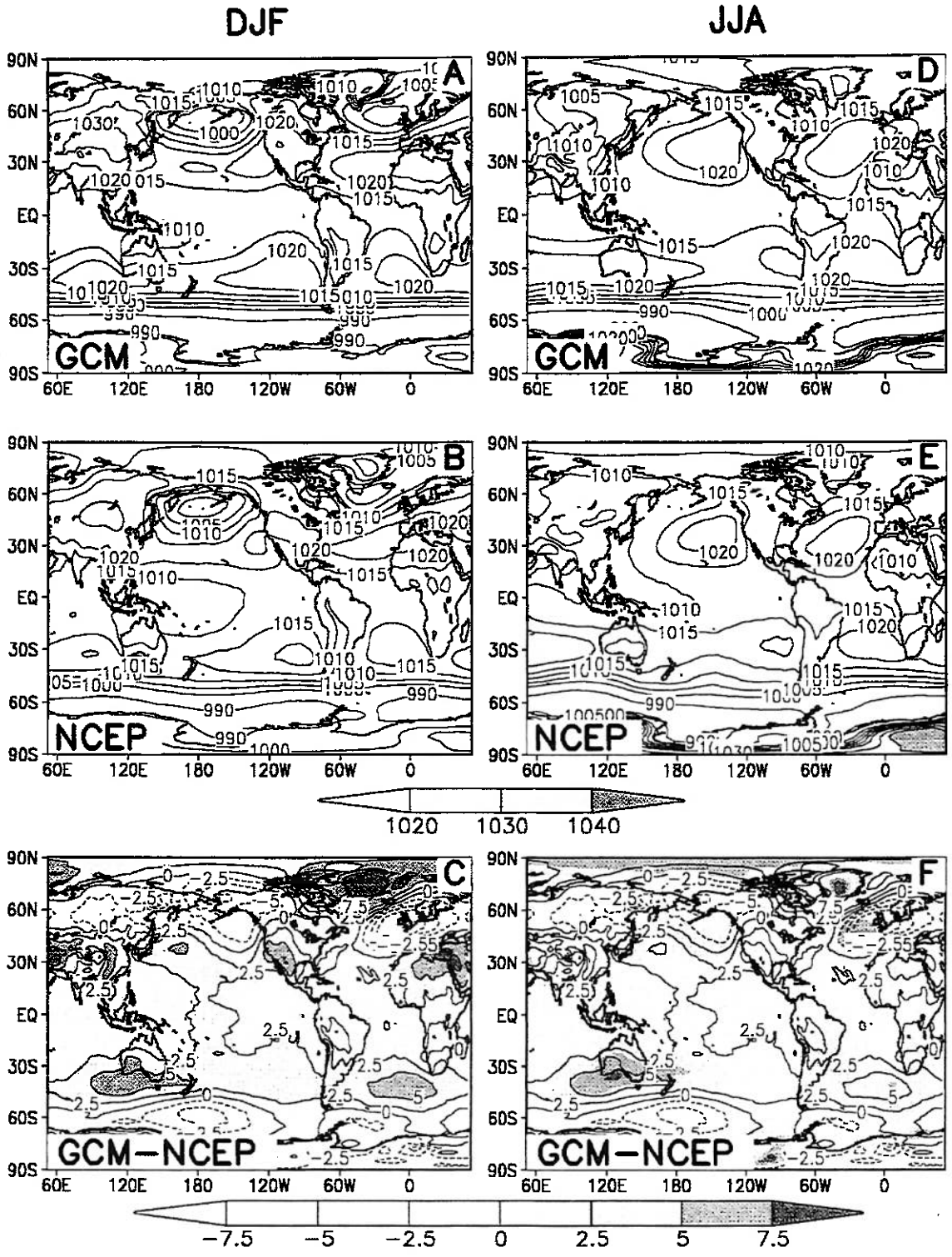

Fig. 3.4 – Climatological sea surface pressure (a) DJF CPTEC/COLA AGCM, (b) DJF NCEP/NCAR reanalysis, d) JJA CPTEC/COLA AGCM, (e) JJA NCEP/NCAR reanalysis, (c), (f) are the differences between the model and observation (hPa).

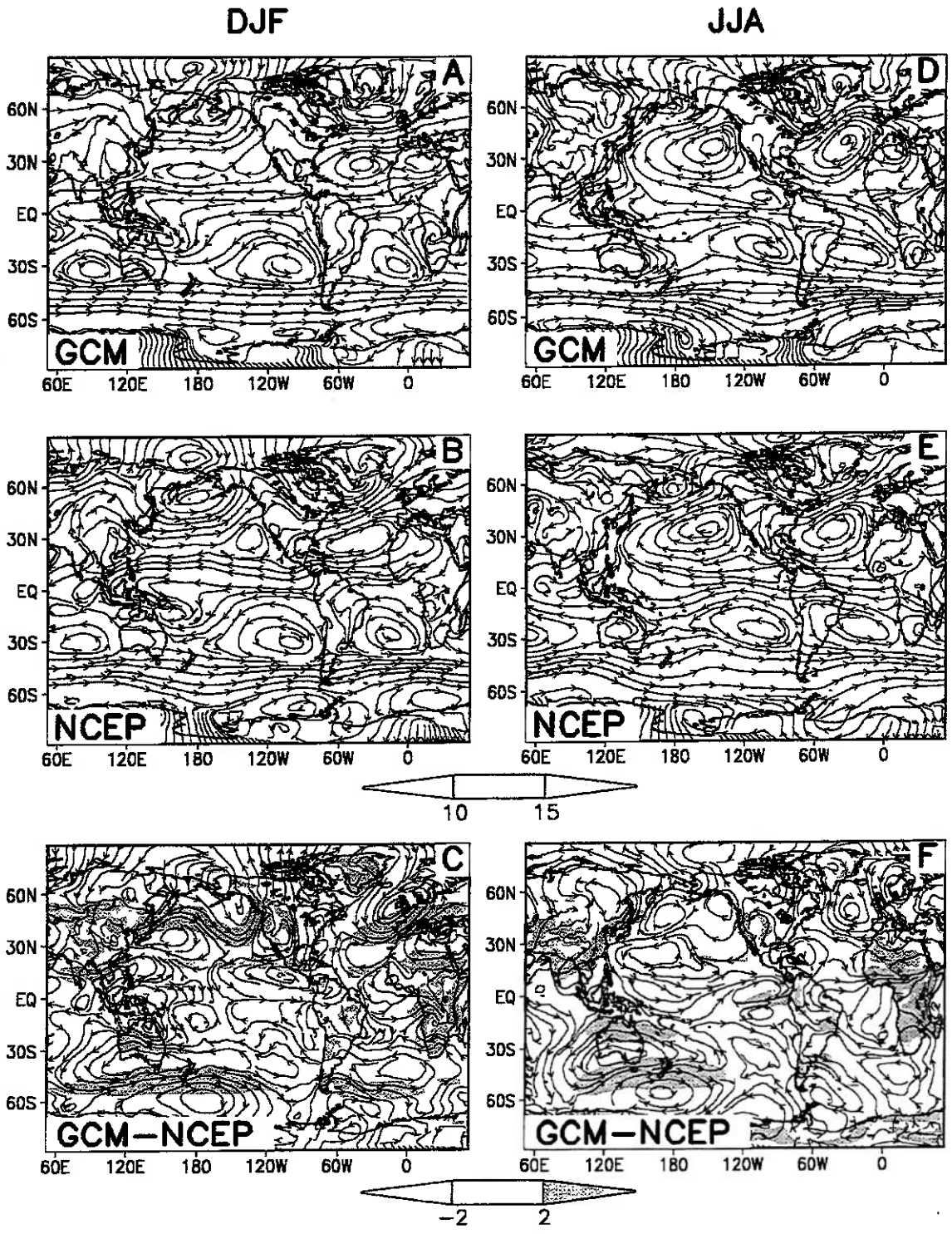

Fig. 3.5 – Climatological wind field at 850 hPa (a) DJF CPTEC/COLA AGCM, (b) NCEP/NCAR reanalysis, (d) JJA CPTEC/COLA AGCM, (e) NCEP/NCAR reanalysis, (c), (f) are the differences between the model and observation ($m.s^{-1}$).

In MAM the Atlantic ITCZ is located in the southernmost position showing its influence on the rainy season of Northeast Brazil (Nordeste). However, the model continues to represent a NW-SE band of precipitation extending from Nordeste to the Atlantic Ocean, linked to the ITCZ and to the convection over Amazonia region, a feature that does not exist in CMAP data (Fig. 3.2d,e). In the observations, the band of precipitation NW-SE is located over Southern Brazil, and is associated with the presence of frontal systems in that region. The model also shows a tilting of the ITCZ towards NE, that gives an overestimation of precipitation in parts of the semi-arid region and an underestimation at the Amazon mouth (Fig 3.2.f).

The Atlantic ITCZ is displaced northwards in JJA but the model still shows large values of precipitation over the northern Nordeste (Fig. 3.2g,h). The reduction of rainfall over large areas of South America is well represented as well as the maximum over the northern region. The main differences over South America occur over the Nordeste region and over Southern Brazil (Fig. 3.2i). The lack of convection over most of South America in JJA is well simulated in the OLR field (Fig. 3.3d-f). This feature is also related to the influence of the Atlantic subtropical high over South America in JJA, when the circulation center is shifted northwards and is closer to the continent than in other seasons (Fig. 3.5d,e). The differences of the South Atlantic Subtropical High between summer and winter are well represented by the model (Fig. 3.5a-f). The South Atlantic Subtropical High is weaker in DJF than in JJA, a feature associated with the development of the SACZ (Satyamurty et al. 1998). The displacement of the South Atlantic High southwards in DJF and the change in the direction of the trade winds in the tropical region are related to the displacement of the confluence zone southwards. This displacement, which also happens in MAM (not shown) is associated with the position of the ITCZ. In JJA the winds are almost parallel to the north coast of Brazil, while in other seasons they have a strong component perpendicular to the coast. These features, which are well simulated by the model, have an implication on the seasonal precipitation variability over the north/northeast coast of South America. The Atlantic trade

winds are weaker in the model than in the observations and this difference can partially be responsible for the excess of precipitation over the Northeasten Brazil.

The convection over Amazonia extends again southeastward in SON, in both model results and CMAP data, but less over Central South America in the model results than in the observational dataset (Fig. 3.2j,k). Instead, the model shows precipitation above 4 $mm.day^{-1}$ over southeastern and part of southern Brazil, while CMAP shows these values only over southern Brazil. However, raingauges data from Brazil stations display a band of precipitation of over 4 $mm.day^{-1}$ extending from the Amazonia to southeast, in this season, that represents the beginning of the interaction between convection over Amazonia and southeastern Brazil precipitation systems. CMAP dataset agrees with Brazil raingauge-based data set in all other seasons. The largest errors between the model and CMAP data are found over the eastern Brazil and over the Andes Cordillera (Fig. 3.2l). The deficit of precipitation over the Amazonia region and excess over the Andes can have an implication on the position and intensity of the anticyclonic circulation at high levels over South America in the Southern Hemisphere summer. In the reanalysis the Bolivian High is concentrated over western South America while in the model results, it is displaced southwestwards over the mountain and amplified in the west-east direction (Fig. 3.6a-c). In the difference field the result is a cyclonic circulation over Amazonia which means less intense anticyclonic circulation associated with weaker diabatic heating due to release of latent heat. The anticyclonic circulation to the east of South America in the difference field can also be associated with the enhancement of the SACZ in the model results and implies in the differences seen in the Atlantic trough at high levels. The flow over South America in JJA is well represented by the model (Fig. 3.6d-f).

Common features over South America in almost all seasons are the excessive precipitation over the Andes Cordillera in the West South America which is related to the deficiency of the model in representing well the orography. The

spurious precipitation anomaly in this region was also found by Stern and Miyakoda (1995) who mention the Gibbs error associated with truncation of steep orography. In JJA when the humidity is very low over Central South America, the model does not produce heavy precipitation over the mountain.

Because of the sigma coordinate, the model does not simulate well the effect of the Andes Cordillera on the flow at low level, as in the reanalysis, but in DJF the flow turns to southeast in the northern part of the mountain, associated with the low pressure over the continent during this season (Fig. 3.5a-c). Another common feature which occurs in almost all seasons is the deficiency of precipitation over Amazonia, Central and Southeastern South America and excess over Northeastern, Eastern and Southern regions of the continent (Fig. 3.2c,f,i,l).

3.2.2 - Features over Africa

The seasonal variability over Africa is identified in the model, with more intense precipitation in DJF, as is seen in the observational data (Fig. 3.2a,b,d,e). However, the model overestimates the values in all seasons over tropical and eastern region. There is a systematic error over the western equatorial region, where a deficit of precipitation is seen in all seasons (Fig. 3.2c,f,i,l). Similar to the simulation over South America, the excess of precipitation over Eastern Africa and defict over the western region affects the high level flow, and the anticyclonic circulation over Southern Africa associated with the summer convection is displaced southeastwards in the model (Fig. 3.6a-c). The North African jet, which occurs in DJF is weaker in the model results than in the reanalysis. The flow in JJA over Northern Africa is also less intense in the model results, but the general characteristics are well represented. In tropical Africa there is less than observed convective activity, but the shift of the convection southwards in DJF and northwards in JJA are noticeable (Fig. 3.3a-f).

3.2.3 - Features over Indian Monsoon region

In the Indian monsoon region, seasonal precipitation variability is also simulated by the model, with maximum precipitation in JJA, although with overestimated values in the southern area and underestimated in the northern area (Fig. 3.2a-f). In the other seasons, there are overestimated precipitation. The Indian monsoon circulation is captured by the model, which shows similar features of the reanalysis field (Fig. 3.5a-f). In JJA there is flow from the Indian Ocean towards India and a small scale trough over the head of Bay of Bengal, features that are very important to the precipitation in this region. Indeed, the model produces intense precipitation during this season. In DJF there are reversed winds over the region in both model and reanalysis fields. The anticyclonic circulation at high levels over the Tibet region, associated with the summer convection in the Northern Hemisphere is well simulated, and is more intense than in the reanalysis (Fig. 3.6d-f). This indicates that the sensible heating is overestimated by the model over the Tibetan plateau.

3.2.4 - Features over Indonesia, Australia and Pacific Ocean

There is a systematic error of precipitation in all seasons over the Indonesia region (Fig. 3.2c,f,i,l). There is overestimation of precipitation over the southern region and underestimation over the northern region. This feature is associated with the position of the SPCZ and to the displacement of the ITCZ northwards. The intensity of precipitation in the southeast part of the SPCZ is overestimated, in all seasons, except in DJF when the model presents an excess of precipitation over Central South Pacific Ocean, related to the zonal extension of this system. Persistent negative errors are displayed in the oceanic area of Indonesia region, extended to the Pacific Ocean while the land areas of this region present positive errors. There is less convective activity than the observations over the region but the different patterns of DJF and JJA are reasonably simulated (Fig. 3.3a-f).

The difference in the winds at low level can contribute to the differences

observed in the Pacific ITCZ pesition. In the Indonesian region and northern Australia the flow at low level is not well represented, mainly in DJF (Fig. 3.5a-f). The differences between the model and reanalysis data show that, similar to the Atlantic, the Pacific trade winds are weaker in the model than in the reanalysis, besides other features associated with differences of magnitude in the westerly regions. Even though, the regions of the strongest winds are well simulated, although with larger values, mainly in the SH. The anticyclonic circulation associated with the North Atlantic Subtropical High in the model results and in the reanalysis presents similar seasonal variability characteristics: moves southwards in DJF and northwards in JJA. The anticyclonic circulation associated with the North Pacific Subtropical High is well represented in JJA when it is intense and in DJF when it is very weak. The South Pacific Subtropical High is well simulated in both seasons.

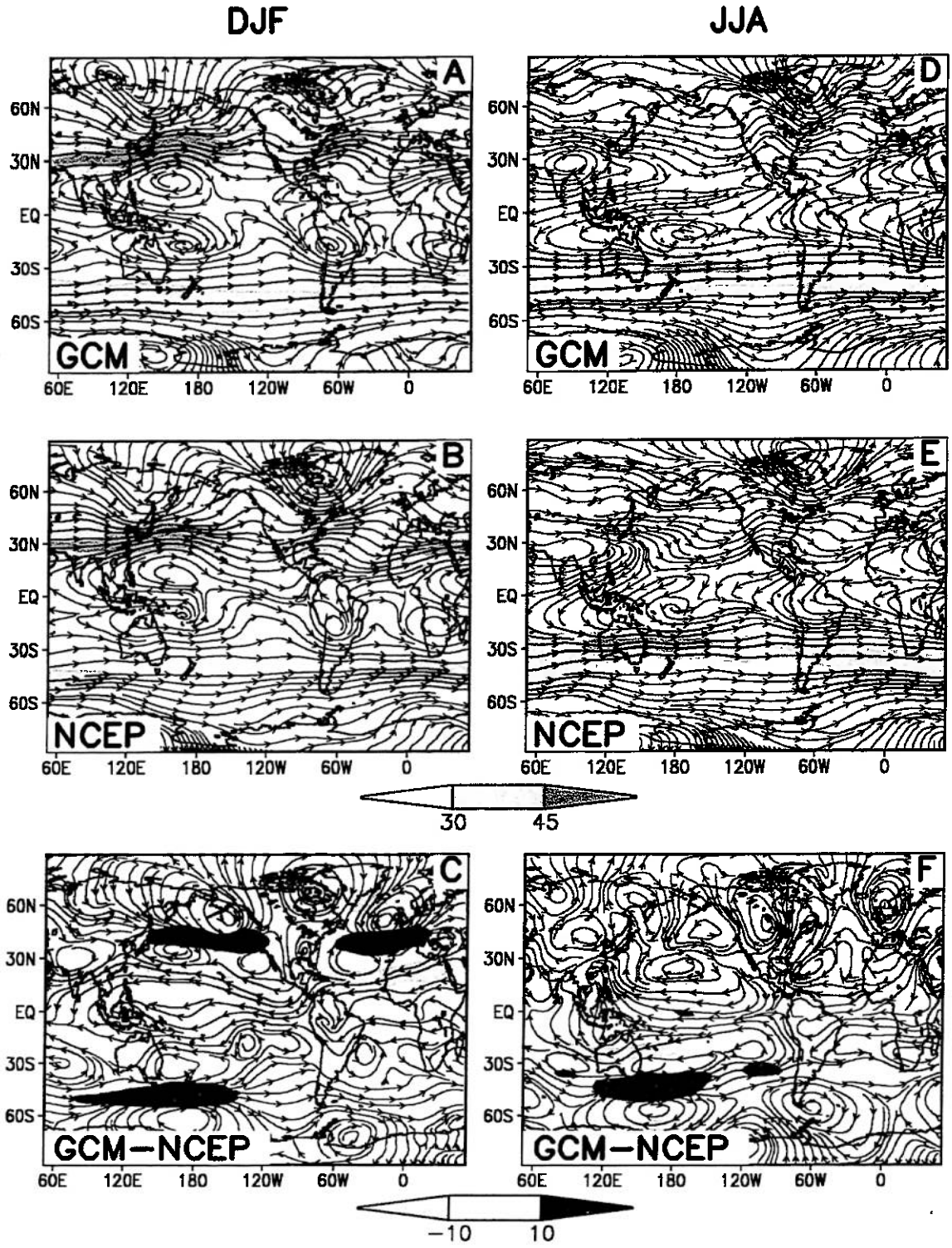

Fig. 3.6 – Climatological wind field at 200 hPa (a) DJF CPTEC/COLA AGCM, (b) NCEP/NCAR reanalysis, (d) JJA CPTEC/COLA AGCM, (e) NCEP/NCAR reanalysis, (c), (f) are the differences between the model and observation ($m.s^{-1}$).

The North Pacific subtropical jet, which is seen in the upper air flow in DJF with its core to the east of Asia, is well simulated (Fig. 3.6a-c). This jet induces anticyclonic and cyclonic circulations at the equatorward side and poleward side over western Pacific Ocean, and this configuration is identified in both model results and reanalysis field. The anticyclonic circulation at high levels over the Western South Pacific Ocean is simulated during the whole year in the model results, associated with the convection over Indonesia. In JJA the model has stronger and more defined anticyclonic circulation over South Pacific Ocean than the reanalysis (Fig. 3.6d-f).

The anticyclonic circulation at low levels over Australia is well represented in all seasons except in DJF when the model has easterly flow over the country, while the reanalysis shows easterlies only over the northern region (Fig. 3.5a,b). The pattern of DJF precipitation over Australia is well simulated, with wet conditions in the northern and northeastern part and dry conditions in the southwestern part (Fig. 3.2 a,b). In this season, the precipitation is overestimated by the model, but in MAM and JJA it is underestimated (Fig. 3.2c,f,i). In SON it is superestimated in the northern and underestimated in the southern Australia (Fig. 3.2l). Light rain rates up to 1 $mm.day^{-1}$ over the subtropical highs and over Australia are well simulated by the model, a deficiency that was found in the intercomparison project models (Lau et al. 1996).

Other climatological feature identified in the model results is the South Pacific trough in DJF that has a different configuration from that shown in the reanalysis, due to the east-west extension of the Bolivian High in the model (Fig. 3.6a-c). In JJA there are zonal westerly winds over the subtropical South Atlantic Ocean and over South America, in both model and reanalysis fields (Fig. 3.6d-f). The model shows strenthening of the winds in JJA, but the Australian jet does not extend over Australia as in the reanalysis, and it is slightly displaced poleward.

3.2.5 - Features over Middle Latitudes of the Northern Hemisphere

The precipitation is also overestimated over Asia and Europe. The model underestimates the precipitation in JJA and SON over large areas of North America and overestimates in DJF and MAM (Fig. 3.2a-f). Over North America the ridge and trough at high levels are well amplified in DJF and displaced eastwards in JJA in both model results and reanalysis data (Fig. 3.6a-f). The strong cyclonic circulation located over northeast North America during both seasons in the reanalysis is well simulated only in JJA. The North Atlantic subtropical jet is identified in the model results in DJF although stronger than in the reanalysis data.

Precipitation associated with storm tracks is simulated in the right regions, over the North Atlantic and North Pacific, mainly in the winter season, DJF (Fig. 3.2a-f). Nevertheless, CMAP data show less intense precipitation than the model results in these areas. In the Southern Hemisphere the model simulates also precipitation associated with storm tracks in the South Indian Ocean extending to the West South Pacific Ocean in all seasons, except in DJF. However, CMAP data does not show comparable values in these areas, but shows in MAM, JJA and SON an area of precipitation over Southern Brazil extending to the South Atlantic Ocean, associated with the occurrence of synoptic systems such as cold fronts and extratropical cyclones. The model represents well this area in JJA.

3.2.6 - Stationary waves

In order to analyze the stationary climatological waves, the zonal means were removed from geopotential height fields at 200 hPa which are shown in Fig. 3.7a-f for the northern hemisphere and in Fig. 3.8a-f for the southern hemisphere. In DJF the model reproduces the dominance of wavenumber two, with two troughs and two ridges, a characteristic feature of the NH winter at mid and high latitudes. The ridge over northwestern North America and the trough to the east of Asia are well simulated, but the trough over eastern North America is

very weak in the model and located over southeastern North America. The center of the ridge over east Atlantic and west Europe, observed in the reanalysis, is displaced eastwards in the model results. The ridge over subtropical Pacific and the trough over North Africa, featuring a wavenumber one in the subtropics, are simulated, although the trough is less intense in the model results than in the reanalysis.

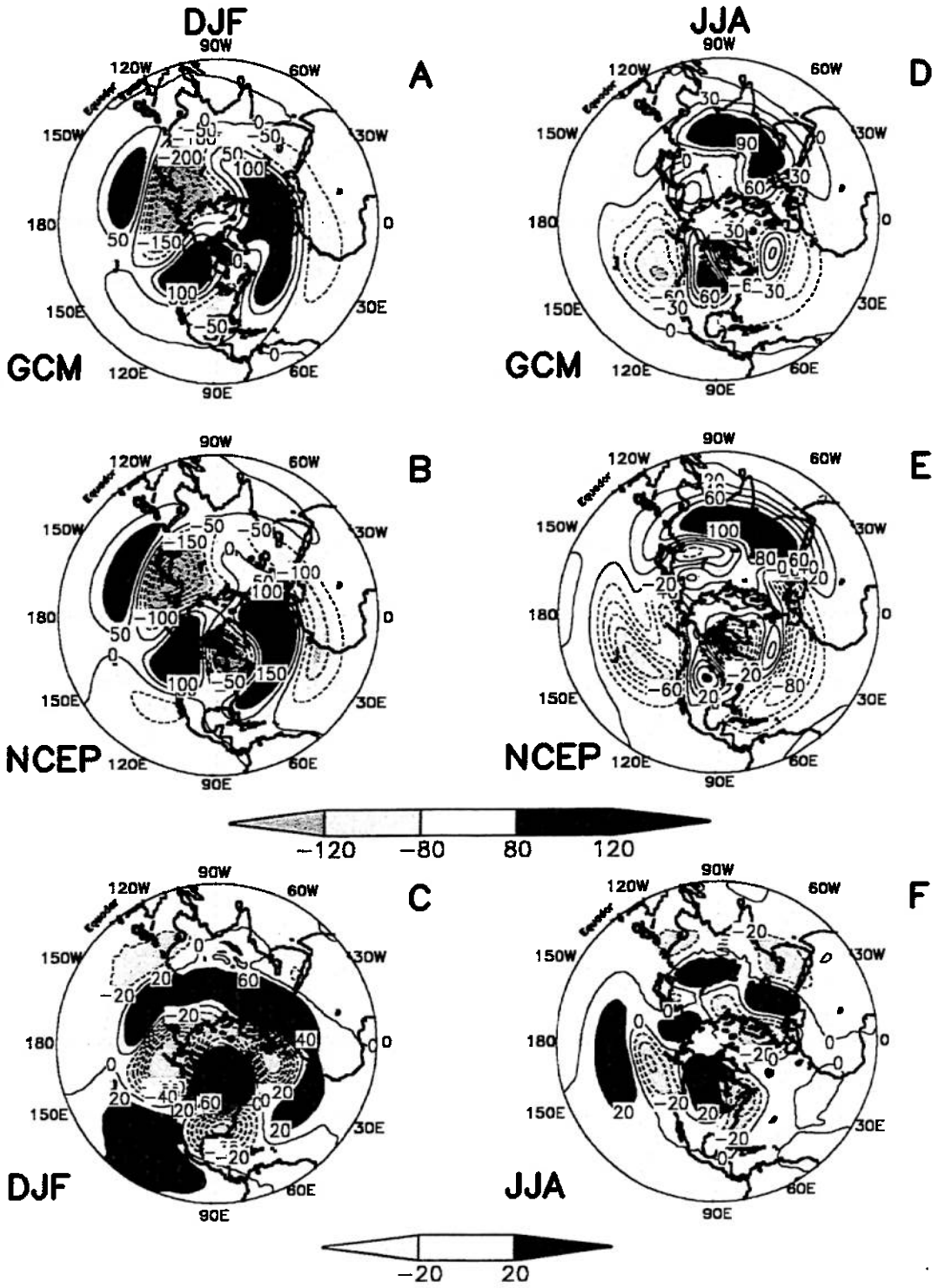

Fig. 3.7 – Climatological zonal geopotential height anomaly at 200 hPa for the Northern Hemisphere (a) DJF CPTEC/COLA AGCM, (b) NCEP/NCAR reanalysis, (d) JJA CPTEC/COLA AGCM, (e) NCEP/NCAR reanalysis, (c), (f) are the differences between the model and observation (m).

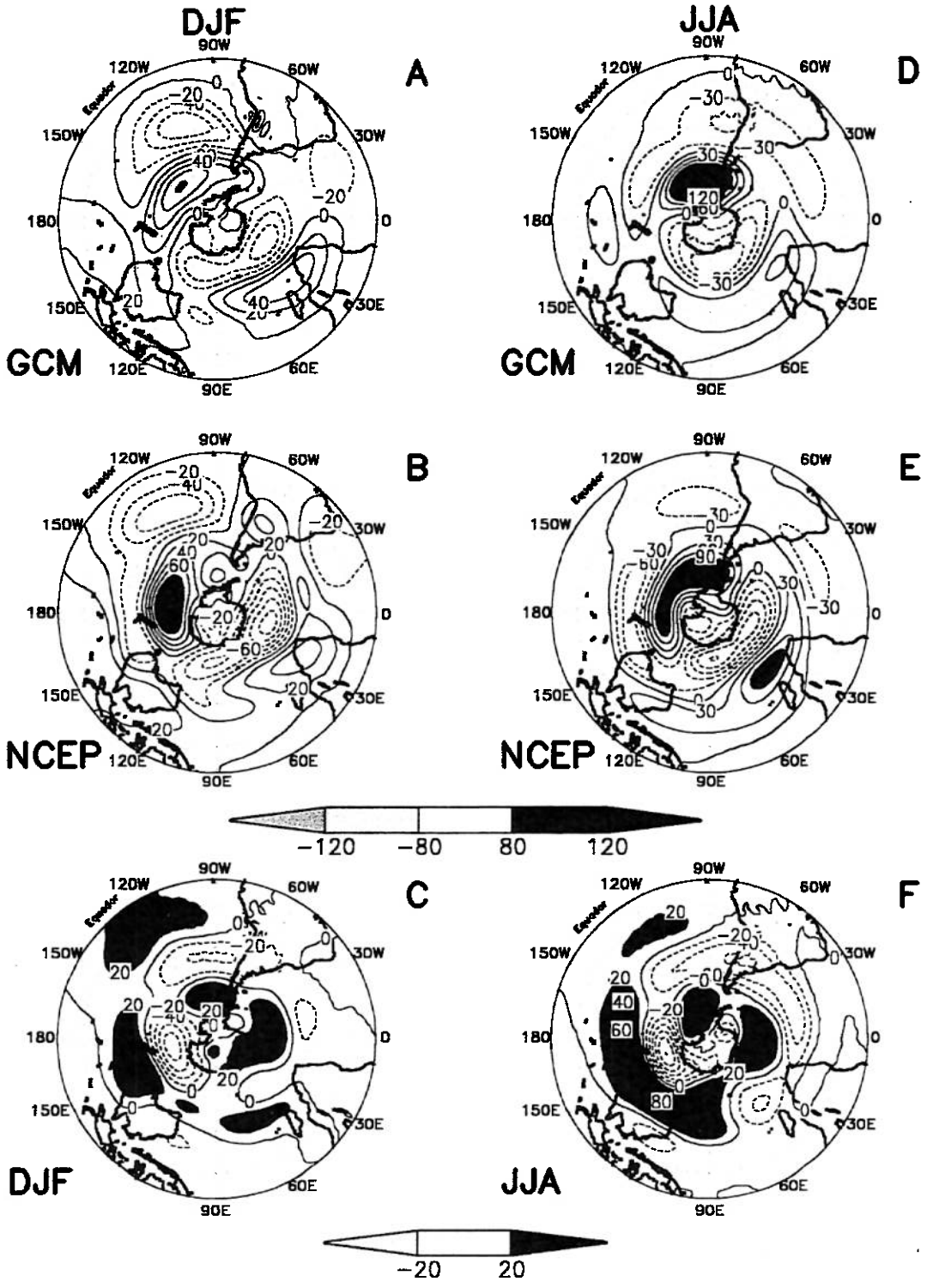

Fig. 3.8 – Climatological zonal geopotential height anomaly at 200 hPa for the Southern Hemisphere (a) DJF CPTEC/COLA AGCM, (b) NCEP/NCAR reanalysis, (d) JJA CPTEC/COLA AGCM, (e) NCEP/NCAR reanalysis, (c), (f) are the differences between the model and observation (m).

In JJA the wavetrain extending from the Western Pacific Ocean over North America to the North Atlantic Ocean is reproduced, with larger intensity than in the reanalysis. The position and intensity of the Tibetan High are well simulated. The intense ridge is related to the strong heating and convection in that region during the NH summer season. These NH winter and summer patterns are also represented in climatological geopotential analyses at 200 hPa, discussed in Wallace (1983). Similar patterns of mid and high latitudes are seen at 500 hPa (not shown). At this level the model represents well the reduction of the zonal anomalies, and the suppression of the high level subtropical features.

In the Southern Hemisphere the wavenumber one observed in the reanalysis in DJF and JJA is reproduced in the model results but there are some differences related to the intensity and position of zonal anomaly centers. The anomalous centers at middle and high latitudes are weaker in the model than in the reanalysis, representing the weaker amplitude of the stationary wave in the model. The ridge over South Pacific is shifted eastwards in DJF when compared to the reanalysis, but in JJA the maximum center close to Antarctica Peninsula is in the right position. In this region the ocurrence of blocking situations is frequent as analysed by Marques and Rao (1999) and Renweek (1998). The ability of the model in representing well the positive geopotential anomaly may indicate that the model is able to simulate blocking occurrences.

At subtropical latitudes the wavenumber one has opposite sign to that at high latitudes and the model presents similar intensities to the reanalysis in DJF but a little displaced eastward. In fact, the whole model pattern is shifted eastwards, showing larger displacement in the South Pacific ridge. The features of the wavenumber one pattern are also identified in the model results at 500 hPa (not shown) with the same displacements as those at 200 hPa. Similar patterns are shown by Raphael (1998), analyzing JJAS quasi-stationary waves in the Southern Hemisphere using NCAR (CCM3) GCM and NCAR Climate System Model (CSM1), which is a coupled atmosphere-ocean model. While the wavenumber one was well depicted by the two models, the wavenumber three

was weak in CCM3 and strong in CSM1. A zonal wavenumber three pattern is also verified in the vertical cross section analysis of the CPTEC/COLA AGCM.

The differences between the model and reanalysis fields of geopotential zonal anomaly in both hemispheres are shown in Fig. 3.7c,f and Fig. 3.8c,f. At high latitudes of the SH large errors occur at the same three regions in both DJF and JJA. At subtropical latitudes, the largest errors occur over eastern and western South Pacific in DJF, and they extend over South America and over south of Australia in JJA. In the NH the errors are larger in DJF, related to the shifting and intensity of the ridges and troughs. The errors in intensity and position of the main centers of the stationary waves may be associated with the poor representation of the model orography.

3.2 MEAN VERTICAL STRUCTURE

3.2.1 Zonal wind

DJF and JJA vertical structures of mean zonal wind from model results and from observations are shown in Fig. 3.9a,b,d,e. The jet streams in the model results are stronger than in the reanalysis data set in all seasons of both hemispheres, except in the NH (JJA) when the model reproduces very well the intensity and position of the subtropical jet. The jet stream centers in the model results are located at the same level of 200 hPa, as in the reanalysis, but they are displaced southwards in the SH when comparing to the reanalysis latitude. However the occurrence of two jets in the SH winter (JJA), one subtropical and another in the stratosphere at extratropical latitudes is depicted by the model. The tropical easterlies at high level are well simulated in JJA, and overestimated in DJF. Overall the differences are larger in the middle and high troposphere in both hemispheres and in the stratosphere of the SH as noted in Fig. 3.9c,f. The circumpolar vortex in the SH summer is too strong compared to the reanalysis. In the improved ECMWF GCM (Brankovic and Molteni 1997) the

zonal wind errors are confined to the upper troposphere and stratosphere. The errors in the troposphere were reduced in the latest version of the model due to the ability of the model in simulating the right position of the NH subtropical jet and the intensity of the SH circumpolar vortex.

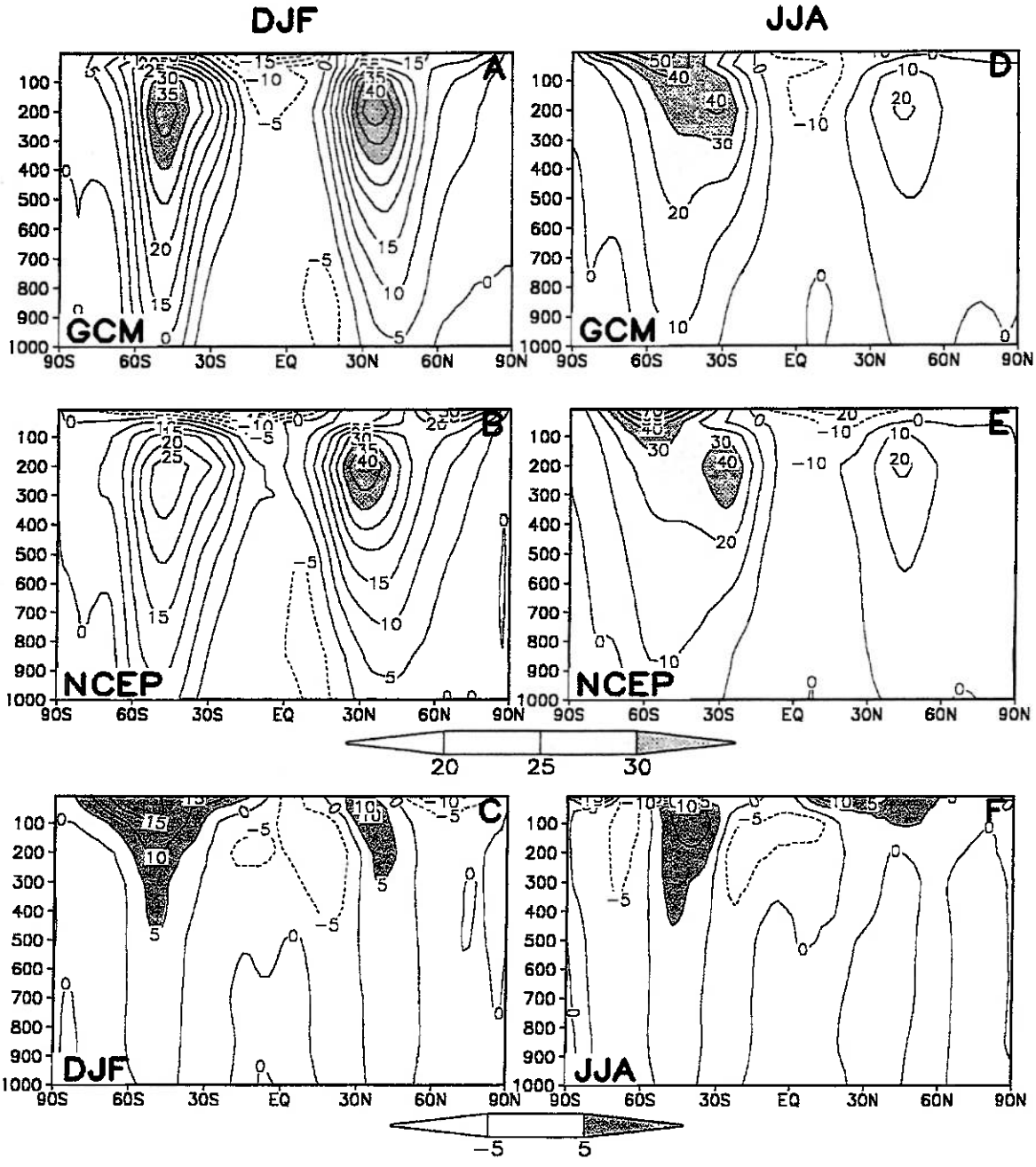

Fig. 3.9 – Climatological vertical structure of zonal wind (a)DJF CPTEC/COLA AGCM, (b) NCEP/NCAR reanalysis, (d) JJA CPTEC/COLA AGCM, (e) NCEP/NCAR reanalysis, (c), (f) are the differences between the model and observation ($.s^{-1}$).

3.2 Meridional wind and meridional circulation

The zonal mean meridional wind in the model results shows very similar behaviour to the reanalysis in JJA (Fig. 3.10d,e). The northward component in the tropics at low levels and southward at high levels are related to the Hadley cell, consistent with the displacement of the tropical heating to the NH in this season. This configuration is also consistent with the cross-equatorial flow in the monsoon region. In DJF the meridional wind associated with the Hadley cell (southward at low levels and northward at high levels) is well represented by the model (Fig. 3.10a,b). The difference fields (Fig. 3.10c,f) show good agreement between the model and reanalysis mean meridional circulation.

The ascent and subsidence associated with the Hadley cell, Ferrel cell and Polar cell are seen in Fig. 11a-d, where the seasonal variation is well detected. In DJF the rising motion in the Hadley cell is located in the tropical SH and the subsidence branch at subtropical latitudes. In JJA the Hadley cell presents rising motion in the tropical NH and subsidence motion over SH subtropical latitudes. The discontinuity observed in the reanalysis in this season is well detected by the model. The difference fields (not shown) indicate slight shifts of the cells and small differences in the intensities between the model and reanalysis.

3.2.1 Air temperature

The general structure of the zonal mean temperature in the model results is comparable to the reanalysis structure (Fig. 3.12a,b,d,e). The seasonal variability in the low troposphere is well detected at mid and high latitudes of the Northern Hemisphere. However, there are differences between the model and reanalysis almost in all levels at subtropical and mid latitudes of the Northern Hemisphere, indicating a cold bias in the troposphere in both seasons (Fig.

3.12c,f). In JJA this cold bias in the NH extends to the high levels of the polar latitudes. The vertical structure of temperature is well simulated in the tropics in both seasons, and in the subtropical latitudes of the Southern Hemisphere in DJF. During this season there are large differences over Antarctica region at high levels and stratosphere, that extend to the middle and subtropical latitudes with a cold bias in both areas. The cold bias, also found in other models such as ECMWF, was reduced in that model, introducing changes in radiation, in cloud parametrization and increasing the vertical resolution (Brankovic and Molteni 1997). However, these changes also introduced a warm bias in the tropical stratosphere. In the Southern Hemisphere winter (JJA) the main differences are found at mid troposphere and stratosphere of the subtropical region and also at high troposphere and stratosphere of the high latitudes. Opposite to the cold bias of the subtropical troposphere in the NH., there is a warm bias in the subtropical troposphere of the SH. Large temperature errors near Antarctica are related to the non realistic response of the model to the orography.

3.3.4 Geopotential height zonal anomalies

The vertical structure of geopotential zonal anomaly is analyzed at 45^0N (Fig. 3.13a-d) and 45^0S, (Fig. 3.14a-d). At 45^0S the reanalysis data show a wavenumber one in DJF and a wavenumber three with barotropic structure in JJA that was not easily identified in the horizontal structure. Although the model captures the wavenumber vertical structure, the anomalies are weak in both seasons.

At 45^0N the wavenumber two is well detected by the model, as well as the vertical structure related to the troughs and ridges, but in DJF the vertical structures of the Eurasian ridge and the Pacific trough are weaker in the model than in the reanalysis. In JJA the geopotential zonal anomalies are stronger in the model than in the reanalysis.

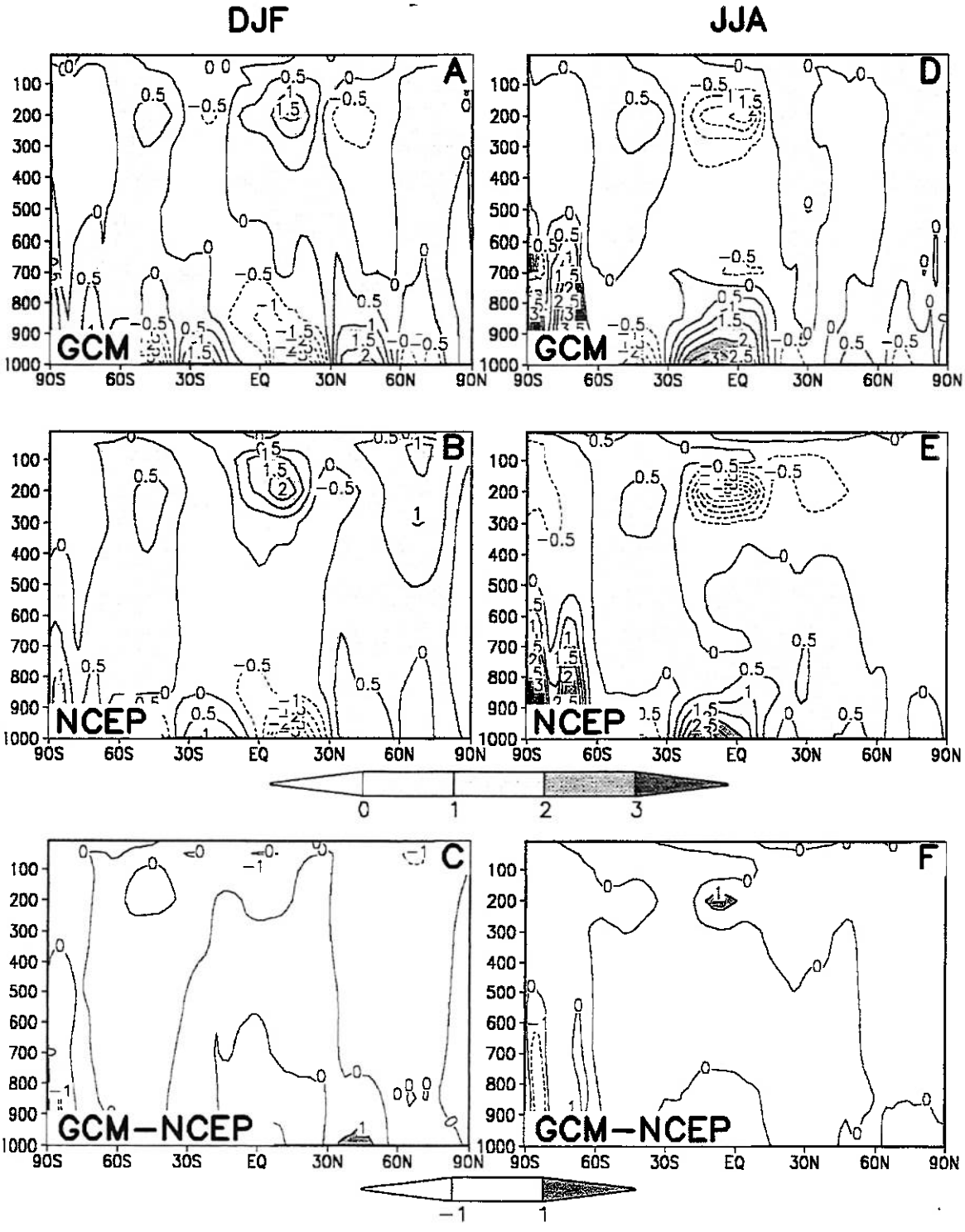

Fig. 3.10 – Climatological Vertical Structure of meridional wind (a) DJF CPTEC/COLA AGCM, (b) NCEP/NCAR reanalysis, (d) JJA CPTEC/COLA AGCM, (e) NCEP/NCAR reanalysis, (c), (f) are the differences between the model and observation ($m.s^{-1}$).

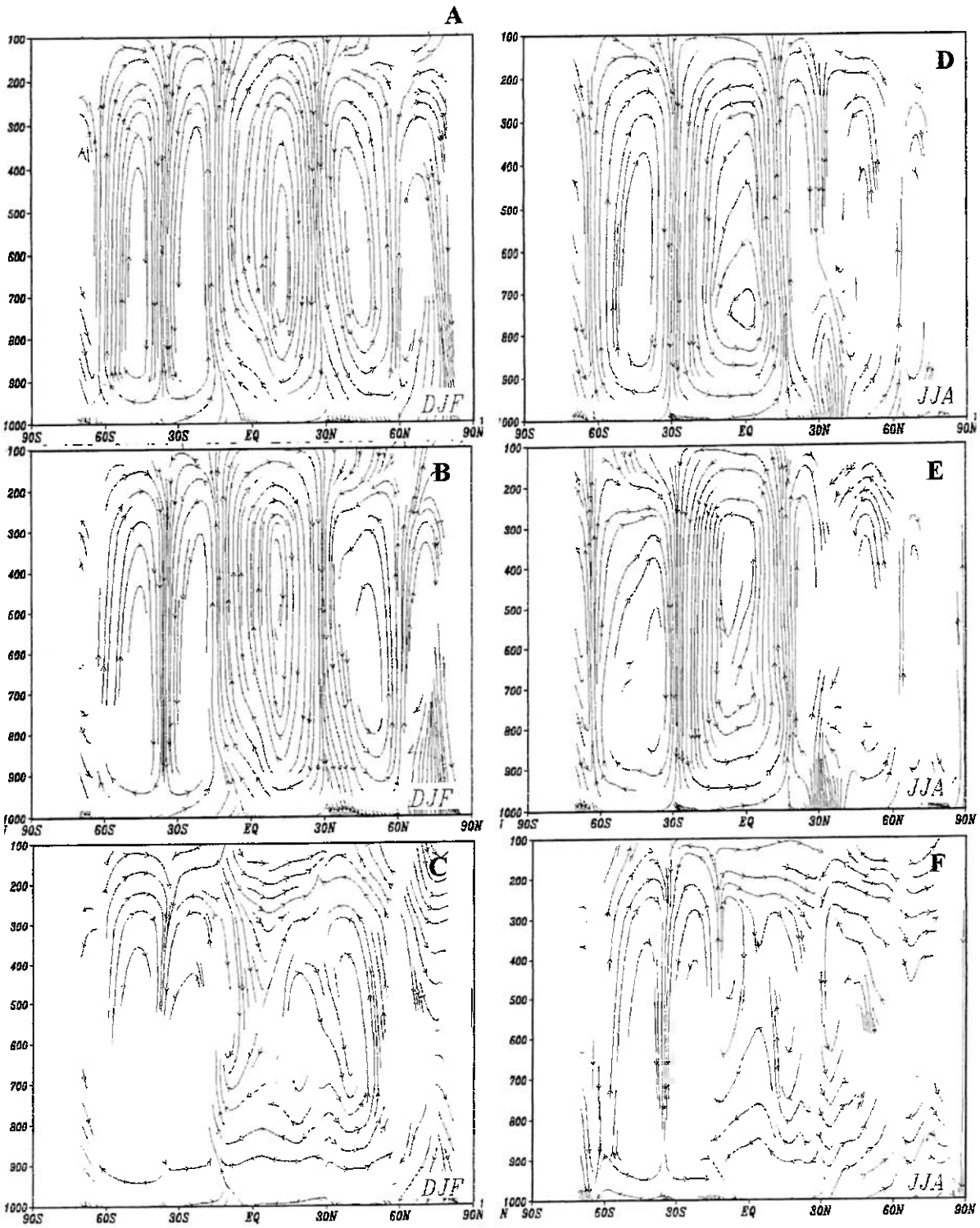

Fig. 3.11 – Climatological meridional circulation (a) DJF CPTEC/COLA AGCM, (b) NCEP/NCAR reanalysis, (c) JJA CPTEC/COLA AGCM, (d) NCEP/NCAR reanalysis ($m.s^{-1}$).

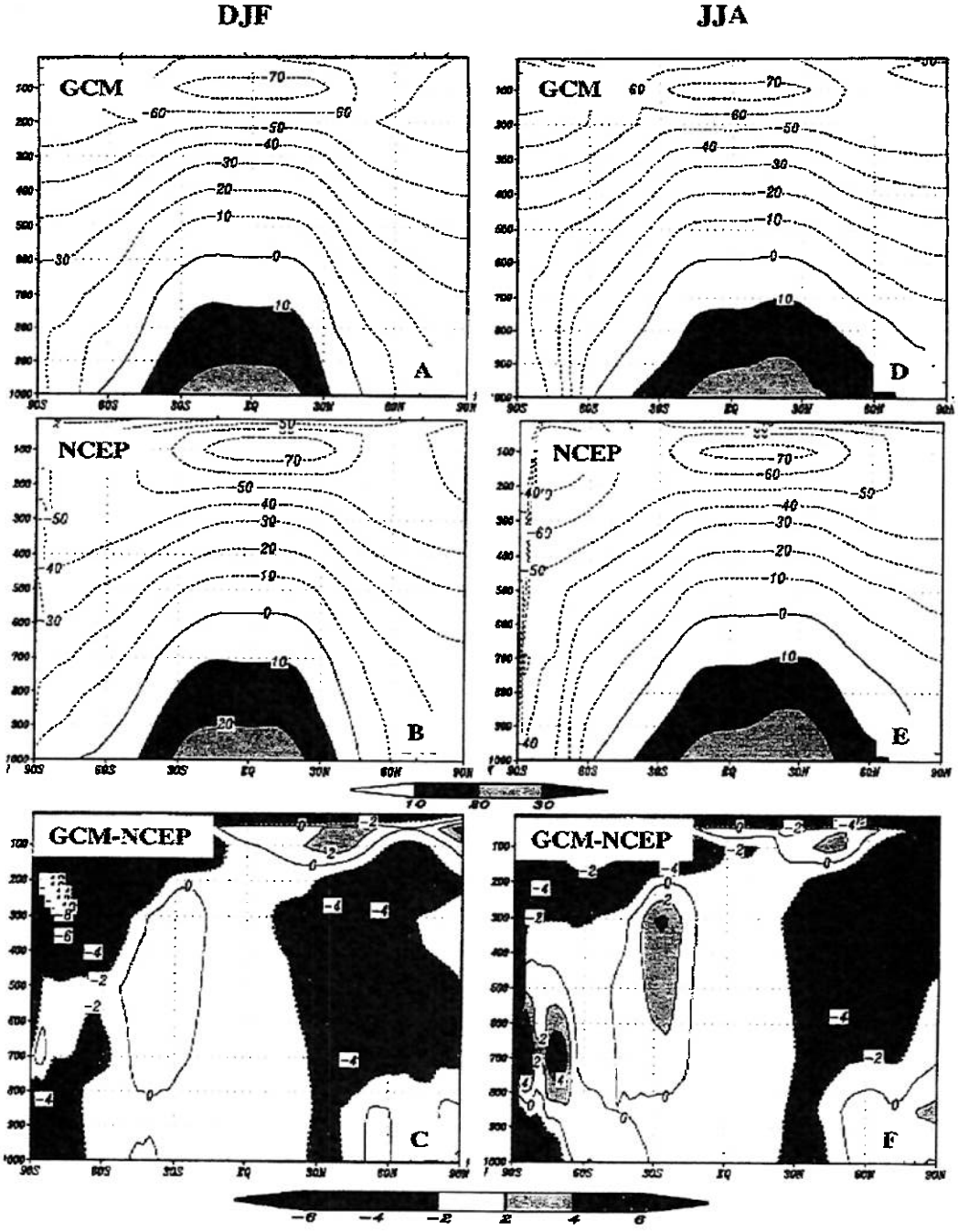

Fig. 3.12 – Climatological vertical structure of air temperature (a) DJF CPTEC/COLA AGCM, (b) NCEP/NCAR reanalysis, (d) JJA CPTEC/COLA AGCM, (e) NCEP/NCAR reanalysis, (c), (f) are the differences between the model and observation (°C).

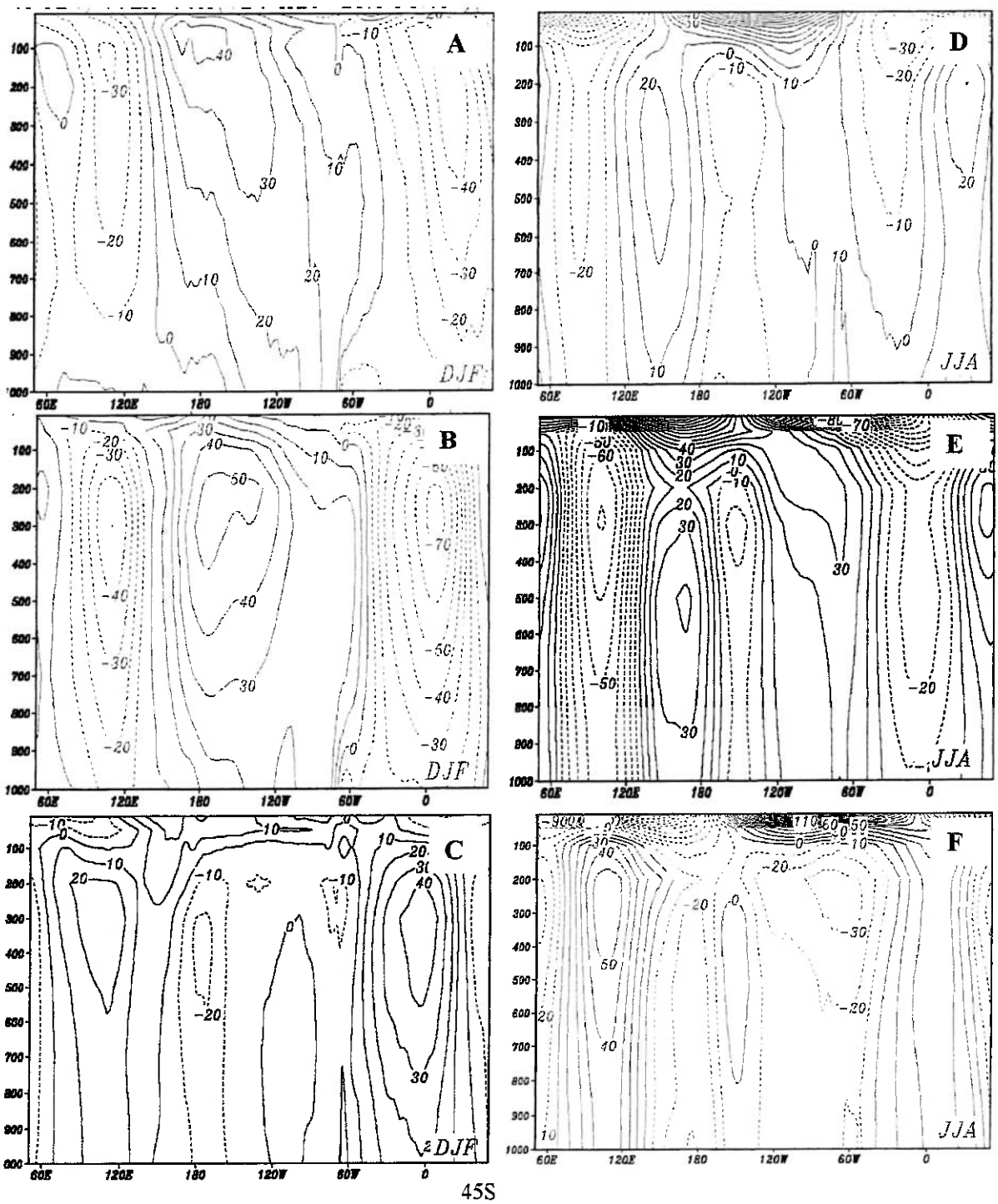

Fig. 3.13 – Climatological vertical structure of geopotential zonal anomally at 45°S (a) DJF CPTEC/COLA AGCM, (b) NCEP/NCAR reanalysis, (d) JJA CPTEC/COLA AGCM, (e) NCEP/NCAR reanalysis, (c), (f) are the differences between the model and observation (m).

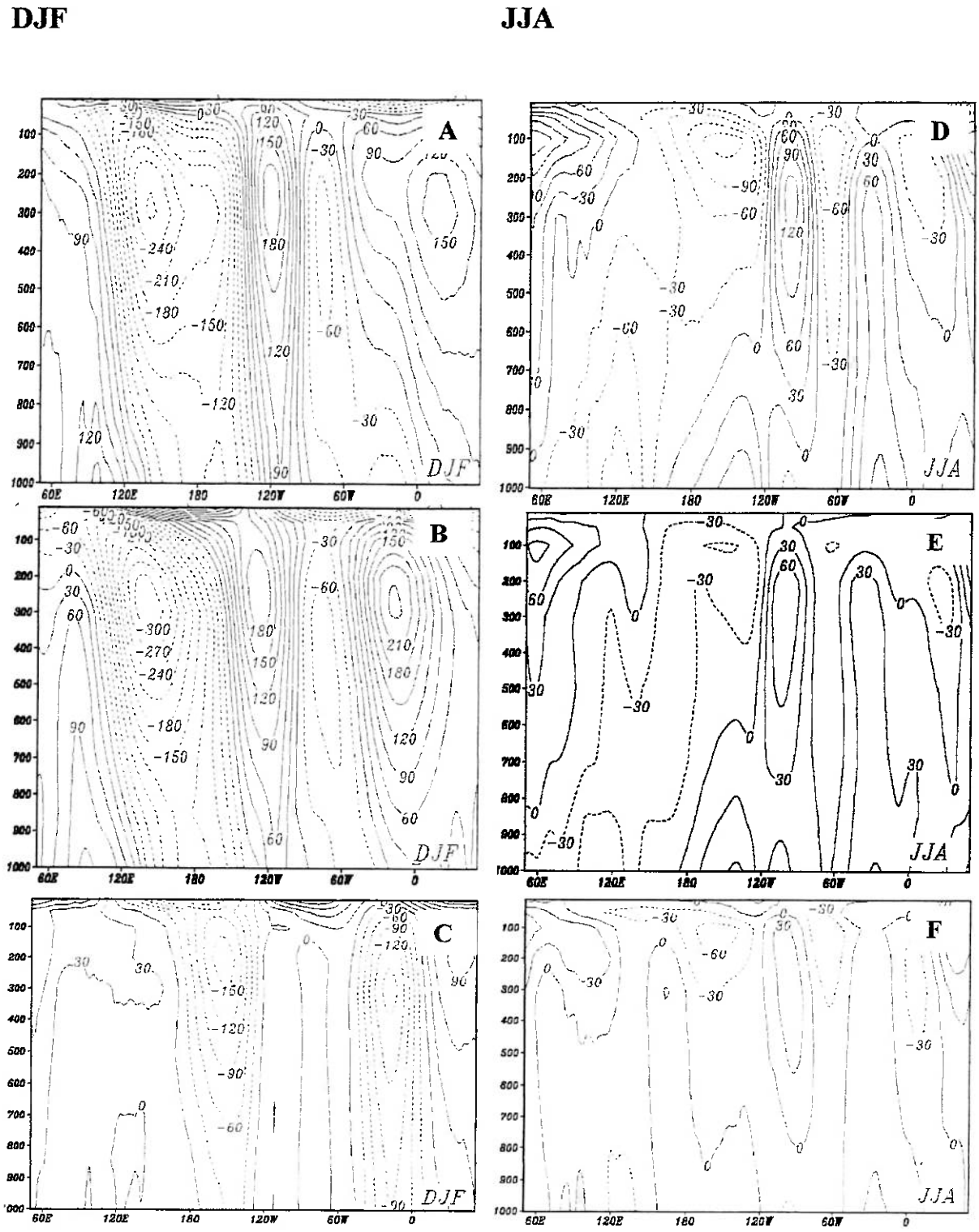

Fig. 3.14 – Climatological vertical structure of geopotential zonal anomally at 45°N (a) DJF CPTEC/COLA AGCM, (b) NCEP/NCAR reanalysis, (d) JJA CPTEC/COLA AGCM, (e) NCEP/NCAR reanalysis, (c), (f) are the differences between the model and observation (m).

3.4 Annual cycle of precipitation of individual members and their mean

The behaviour of the nine-member ensemble related to the monthly mean precipitation is discussed by analysing the average land precipitation over the Northern and Southern Hemispheres and over continental areas shown in Fig. 3.15. CMAP data, the ensemble mean and the results of each integration are shown in Fig. 3.15a-l. Northern and Southern Hemisphere results show the simulation of the opposite annual cycles, although the precipitation is overestimated in the northern hemisphere during the whole year (Fig. 3.15a,b). In the Southern Hemisphere the simulation results are also overestimated but they are close to the observations in June and July. In both hemispheres the members show a consistent behaviour, making the ensemble mean a representative value of the simulation.

Over South America there is also consistency among members (Fig. 3.15c). Values close to observations occur in March and April. In other months the model overestimates the precipitation, but the maximum in summer months and minimum in winter months are noticeable. The dispersion among members in North America is small(Fig. 3.15d). The ensemble shows values close to observations in July, August and September and the smooth seasonal variation is well represented by the model.

The model also overestimates precipitation over Europe and Scandinavia, (Fig. 3.15e), but simulates well the values in August. The larger dispersion over this area than that over North and South America can be related to the smaller analyzed area, however, the dispersion is less than 0.25 $mm.day^{-1}$. The dispersion in Africa and Middle East results is very small, but the precipitation is overestimated during the whole year, with deviations from the observed values larger than in the other continents (Fig. 3.15f). In the northern sector of Africa and in the Middle East the seasonal variability is very low, and therefore the annual cycle of the whole region, north and south of equator together,

represents the seasonal variability of the southern portion. The model shows a more intense annual cycle than observations. In Sahel there is consistency among members and the model simulates extremely well the values and the seasonal variability (Fig. 3.15g). The annual cycle is well simulated in the Asia region, but the model also overestimates the values (Fig. 3.15h). Over India and South Asia the simulated values are closer to observations in August and September (AUG-SEP), and higher in other months (Fig. 3.15i). The similarity in AUG-SEP shows the ability of the model in representing well the later part of the rainy season related to the India monsoon. Dispersion among members in Australia is larger in DEC-FEB, when the model overestimates the values, than in other months when the model results are similar to the observational data (Fig. 3.15j). In the Indonesia region, taking only the land precipitation, the model overestimates the observed values and gives an annual cycle stronger than the observed (Fig. 3.15k). Taking the land and ocean precipitation of the maritime continent, the model shows underestimated values but very close to the observations in almost all months (Fig. 3.15l).

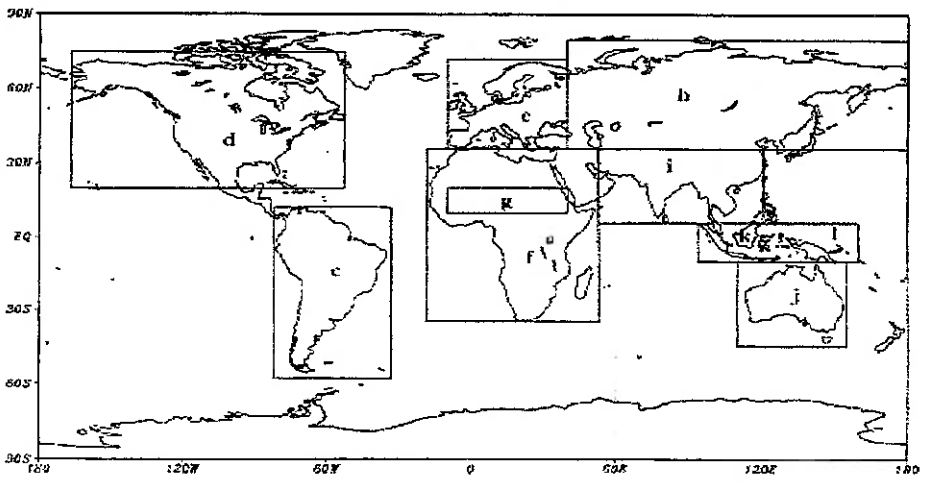

Fig. 3.15 – Areas for the analysis of monthly spatial average precipitation considering all ensemble members and CMAP data. Only land values are considered in the spatial average. (a) Northern Hemisphere, (b) Southern Hemisphere, (c) South America, (d) North America, (e) Europe and Scandinavia, (f) Africa and Middle East, (g) Sahel, (h) Asia, (i) India and South Asia, (j) Australia, (k) Indonesia, (l) Indonesia (land and ocean) ($mm.day^{-1}$).

(continue)

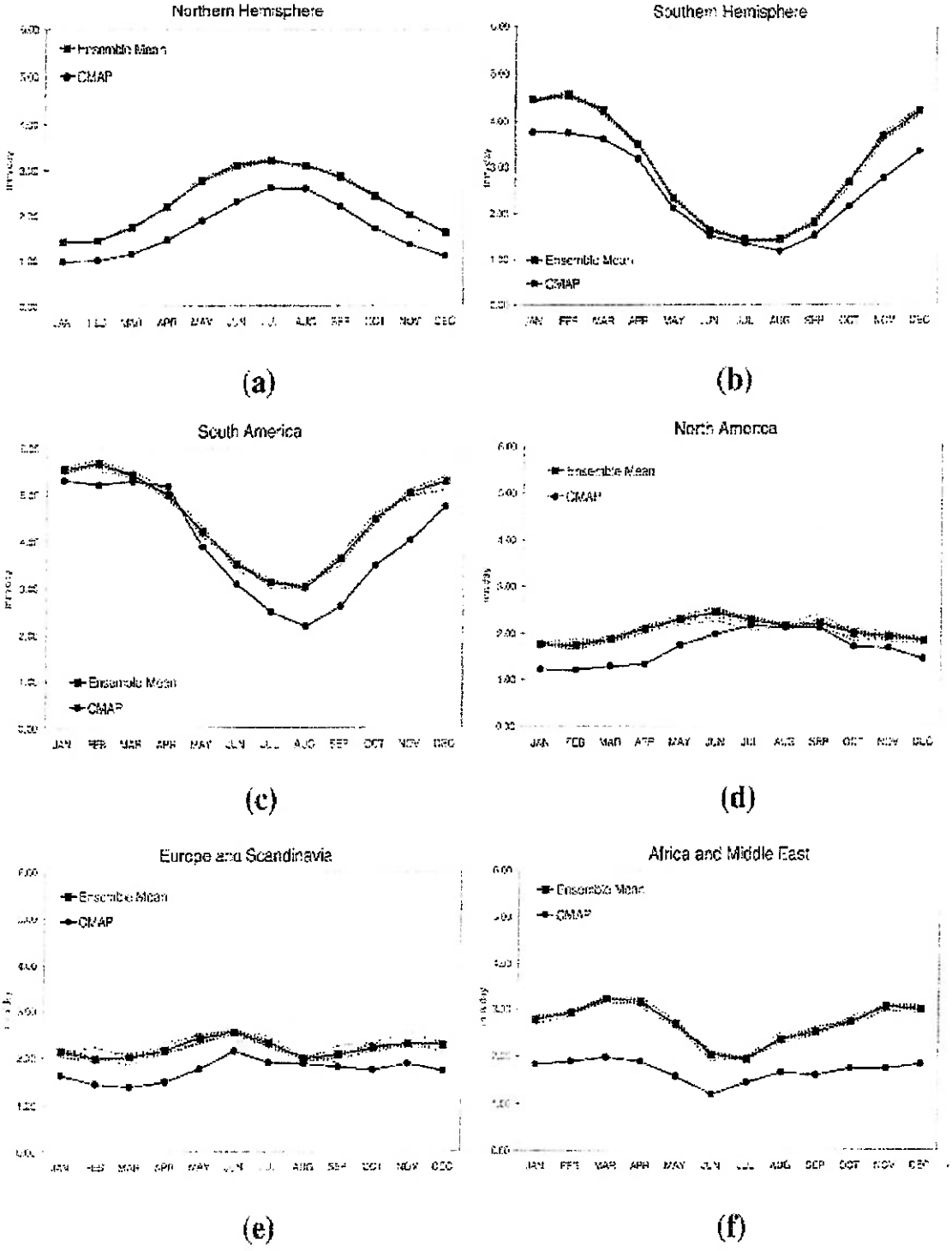

Fig. 15 (continue)

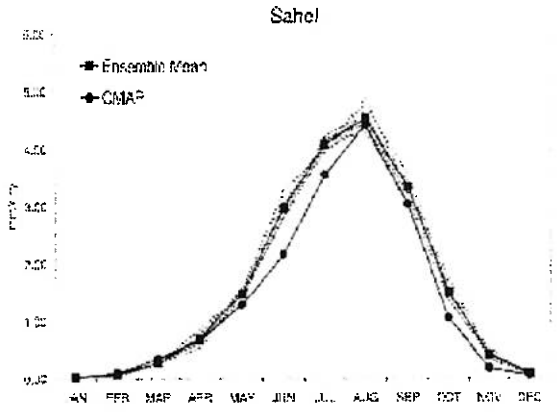

(g)

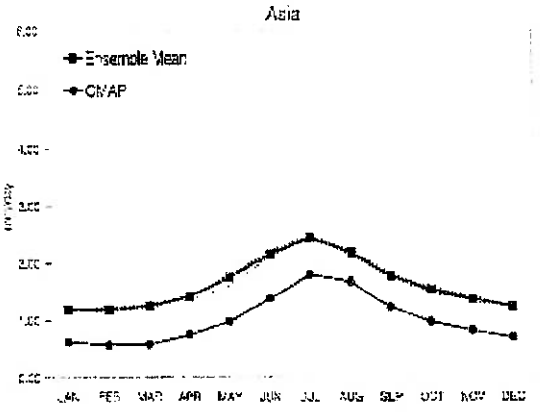

(h)

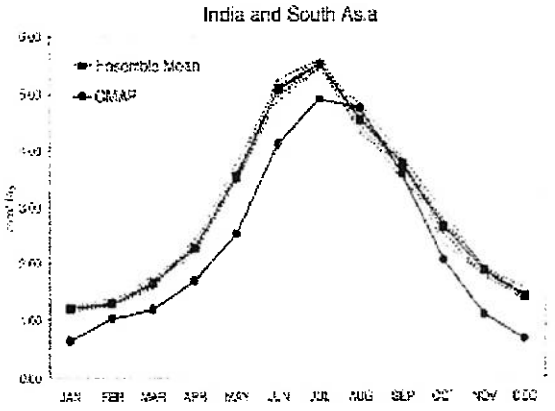

(i)

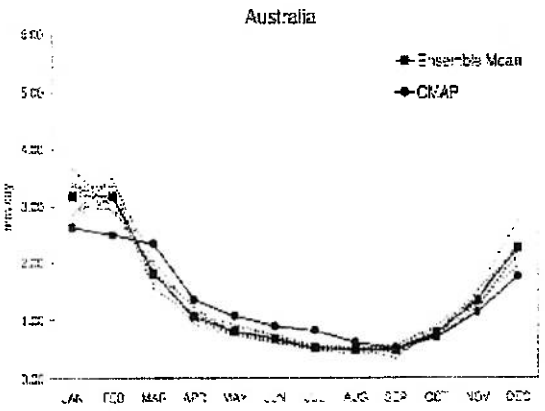

(j)

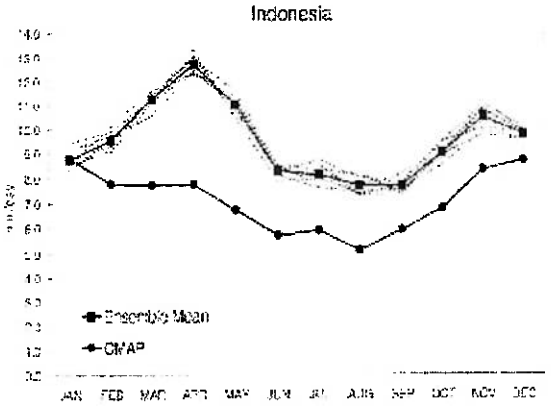

(k)

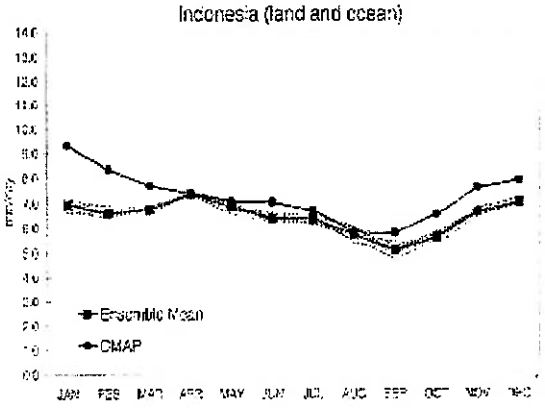

(l)

Fig. 15- (end)

Consistency among members is also found even when smaller areas are considered. As an example, some areas over South America, shown in Fig. 3.16, are analyzed. Overestimated values occur over northern Northeast Brazil in all months, the values being similar in December and March (Fig. 3.16a). The annual cycle is smoother than the observational cycle and the dispersion is larger from January to July than in other months. Close values in March and April show the ability of the model in representing the rainy season of northern Northeast Brazil. In southern Northeast Brazil the dispersion among members is larger than in the northern portion in March, April and May (Fig. 3.16b). However, in other months the ensemble mean represents well the behaviour of the members. The ensemble values overestimate the observational data, with larger differences from January to July. Here, the same area is taken for both northern and southern Northeast Brazil.

The Amazon region is well simulated from JUN-NOV, but there are large underestimated values in other months (Fig. 3.16c), when the observed convection is intense over southern Amazonia. However, there is consistency among members during the whole year. The model shows similar values to the observations in Southeast Brazil from May to September, when there is also convergence among members (Fig. 3.16d). In the rainy season of this region, from late spring to summer, the model overestimates the observed values and the dispersion is higher than in winter. In the spatial analyses (Section 3.2) the precipitation of this region was associated with a more intense SACZ in the model results. In central South America the model values are very close to the observations (Fig. 3.16e).

There is consistency among members in northwest Peru and Equador and similar values in June and July, but there are overestimated values from February to May (Fig. 3.16f). The model behaviour in this region is opposite to that in the Amazon region, where the model shows underestimated values during this period. As mentioned before, these errors may be connected

through excess of convection/ascent movement over Northwest South America and deficit of convection/subsidence movement over Amazon region (direct thermal circulation). The annual cycle has also opposite behaviour.

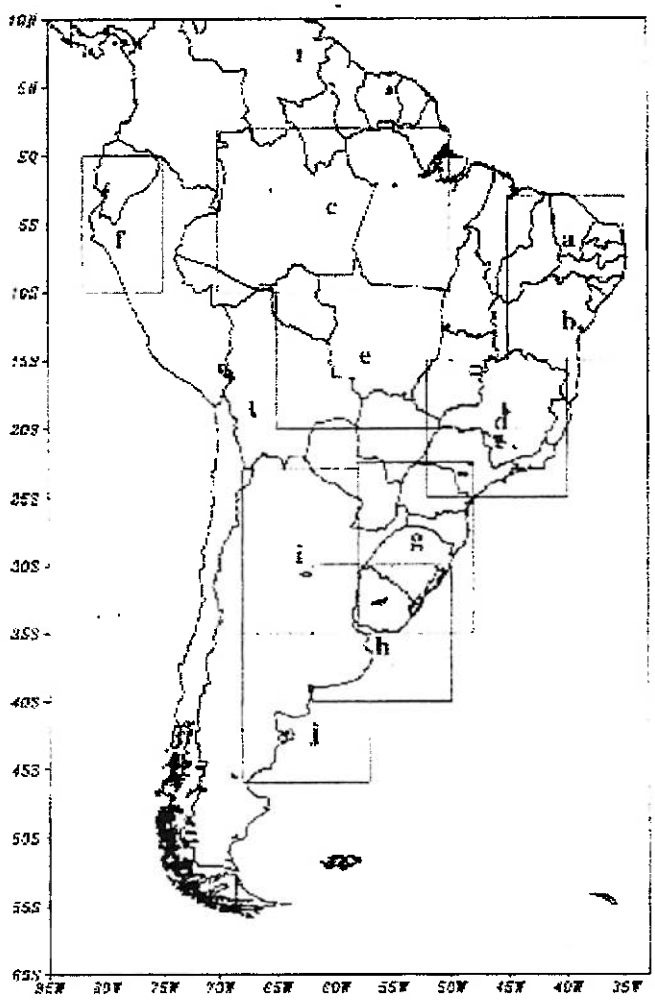

Fig. 3.16 – South America areas for the analysis of monthly spatial average precipitation considering all ensemble members and CMAP data. Only land values are considered in the spatial average. (a) Northern Nordeste, (b) Southern Nordeste, (c) Amazonia, (d) Southeast Brazil, (e) Central South America, (f) Northwest Peru and Equador, (g) Southern Brazil, Uruguay, Eastern Paraguay, (h) Southern Brazil, Uruguay, Eastern Argentina, (i) Northern Argentina, (j) Southern Argentina ($mm.day^{-1}$).

(continue)

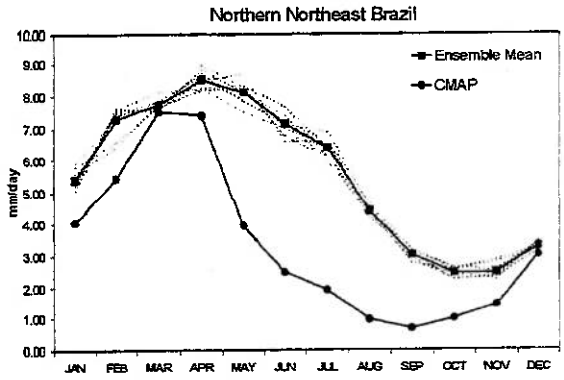

(a)

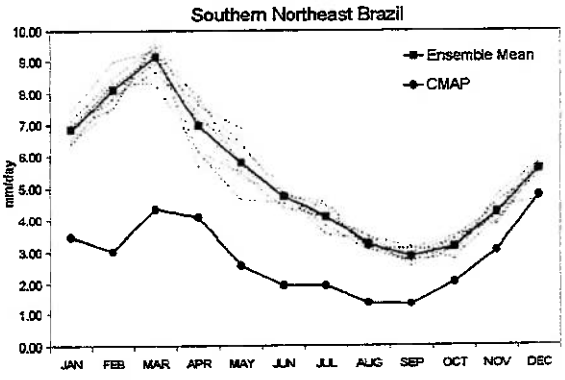

(b)

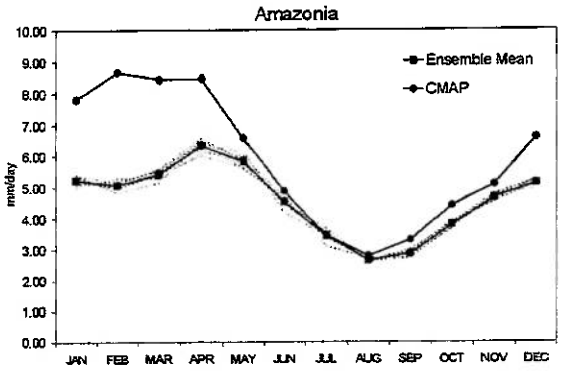

(c)

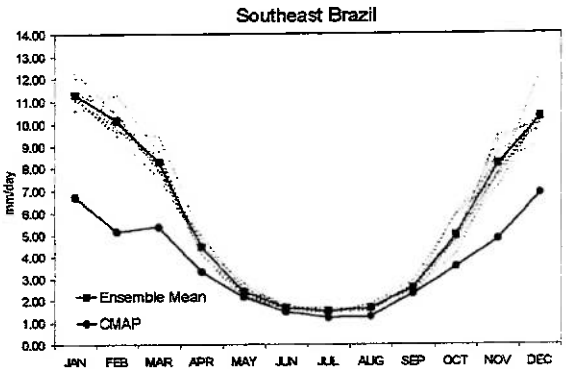

(d)

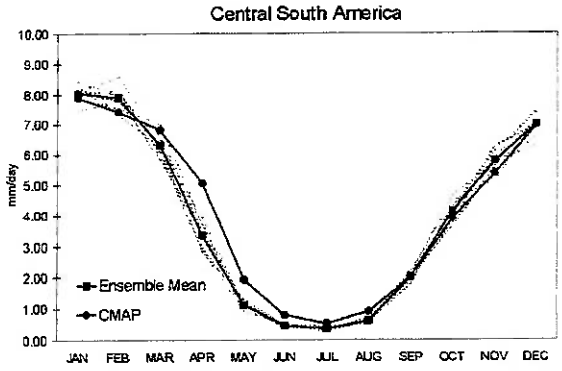

(e)

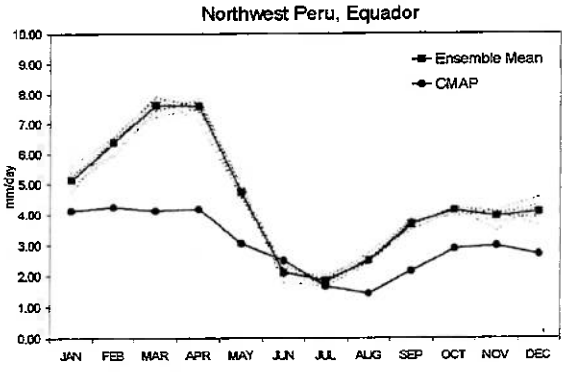

(f)

Fig.3.16- (continue)

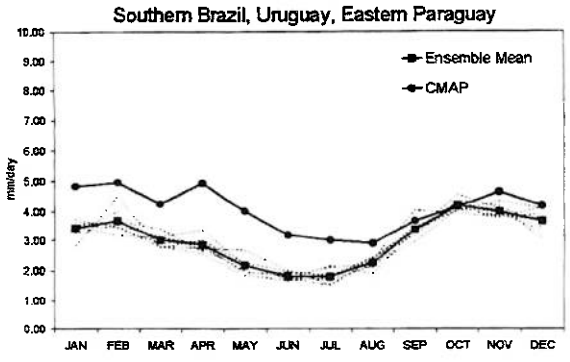

(g)

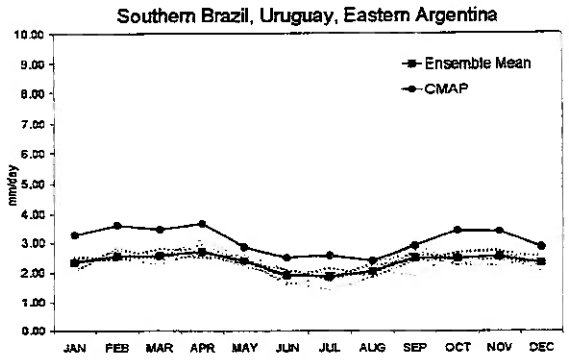

(h)

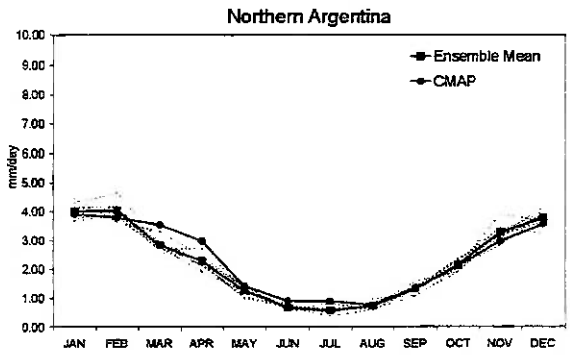

(i)

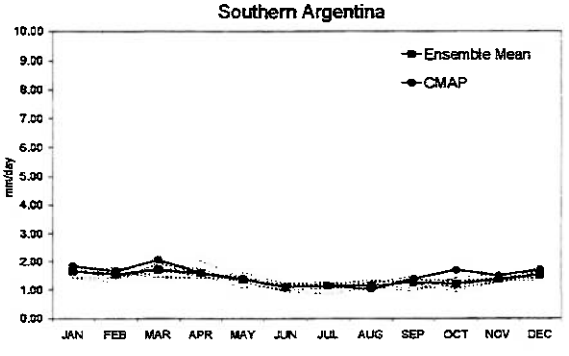

(j)

Fig. 3.16- (end)

In Peru/Equador the annual cycle is stronger and in Amazonia is weaker in the model than in CMAP data set. There are underestimated values in the area which comprises southern Brazil, Uruguay and eastern Paraguay in all months except in October (Fig. 3.16g). The dispersion in winter among ensemble members is smaller than in summer. Another area which presents lower values than the observations is the southernmost of Brazil, Uruguay and eastern Argentina (Fig. 3.16h), but the values are very close. The ensemble mean represents well the observed values over northern and southern Argentina (Fig. 3.16i,j). These are the regions in South America where the model showed, in all months, closer values to the observations than over the other analyzed regions.

3.5 ENERGY BUDGET

The global energy budget is presented in Tables I and II, which contain model results and observational estimates from Kiehl and Trenberth (1997). The budget is analysed at the top of the atmosphere and at the surface.

Table 3.1 shows that the net shortwave radiative flux (SW) at the top of the atmosphere is larger in the model than in the observations by 14 Wm^{-2} in all-sky conditions and by 9 Wm^{-2} in clear-sky conditions. The difference is related partially to the underestimation of the cloud fraction in the model (10% less cloud cover) and to the subsequent underestimation of the SW cloud radiative forcing. The neglect of the aerosol effect in the model as well as the underestimation of the surface albedo (4% lower than the climatological value) also contribute to the difference.

A better agreement is obtained between the simulated and the observed values of the upward longwave radiation (OLR). The difference is about 3-4 Wm^{-2} in both all-sky and clear sky conditions. Note that the longwave cloud radiative forcing is simulated accurately. The model shows larger values of OLR but, as mentioned, not enough to balance the incoming SW radiation at the top of the atmosphere. This is partially due to gaps in the SW and LW radiation schemes and probably due to the fact that the model SST is prescribed in the model and does not respond to the solar radiation input. In the spatial OLR analyses, section 3.2, larger values in the model than in the observational data were found in regions of the subtropical highs, and it was speculated that the problem could be related to the influence of low level clouds on the radiation process.

TABLE 3.1 - ENSEMBLE GLOBAL ANNUAL ENERGY BUDGET AT THE TOP OF THE ATMOSPHERE (TOA). Shortwave (SW) and longwave (LW) radiative fluxes and cloud radiative forcing are in Wm^{-2}. Cloud fraction and albedo are displayed in percent.

	OBSERVED	CPTEC/COLA
SW downward	342	341
SW NET	235	249
SW clear-sky NET	286	295
Albedo	31%	27%
OLR	235	239
OLR clear sky	265	268
SW upward	107	92
Cloud fraction	62 %	53%
SW cloud forcing	-51	-46
LW cloud forcing	29	29
Net TOA	0	10

The surface radiation budget is presented in Table 3.2. The model overestimates also the net shortwave radiative flux at the surface in both all-sky and clear-sky conditions by 22-23 Wm^{-2}. This is related to the overestimation of the downward shortwave flux in the clear-sky conditions (about 9 Wm^{-2}), underestimation of the surface albedo value (contributing to a larger SW absorption of about 8.5 Wm^{-2}) and to the magnitude of the cloud fraction. The net longwave radiation in the model is underestimated by 3 Wm^{-2}, latent heat flux is overestimated by 24 W m^{-2}, and sensible heat flux is underestimated by 4 Wm^{-2}. Overall there is an excess of SW energy of 6 Wm^{-2} which is not balanced by longwave, latent and sensible heat (SW= LW+LH+SH). This imbalance is probably due to the lack of interaction between ocean and atmosphere caused by the continuous forcing of the SST. The error in the model results can also be related to the amount of tropospheric aerosol. The addition of tropospheric aerosol in the NCAR/CCM3 GCM improved the clear sky SW radiation (Kiehl et

al. 1998).

TABLE 3.2- ENSEMBLE GLOBAL ANNUAL SURFACE ENERGY BUDGET. Shortwave (SW) and longwave (LW) radiative fluxes, latent and sensible heat fluxes are displayed in Wm^{-2}, precipitation in mm/day and precipitable water in mm.

	OBSERVED	CPTEC/COLA
SW NET	168	191
Clear sky SW NET	217	239
LW upward	390	398
LW downward	324	335
LW NET	66	63
Clear sky LW upward	390	398
Clear sky LW downward	278	307
Clear sky LW NET	112	91
Latent Heat	78	102
Sensible Heat	24	20
NET surface	0	6
Precipitation	2.7	3.5
Precipitable Water	25.5	23.9

Over the continent the imbalance is about 3 Wm^{-2}, while over the ocean it is about 8 Wm^{-2}. The larger latent heat flux implies larger evaporation, and the excess of humidity leads to larger global precipitation, since the model precipitable water is even less than the observed value. The imbalance may be also due to the existing deficiencies in the numerical schemes to calculate heat fluxes. The Bowen ratio calculated over land is 1.0 in the model, compared to the observed value of 0.96, although both latent heat and sensible heat fluxes are higher in the model. However, over the ocean, the Bowen ratio is 0.09, while the climatological value is 0.11. This difference is due to the higher latent heat over the ocean in the model (124 Wm^{-2}), against 98 Wm^{-2} calculated in climatological analysis of Baumgartner and Reichel (1975). The

sensible heat flux over the ocean is 11 Wm^{-2} in the model and in the climatology.

The present analysis indicates that the SW radiative transfer code employed in the model needs to be improved as well as the cloud cover scheme. The parametrization of evaporation over the ocean also needs a revision. A more detailed discussion of the energy budget simulated by the model will be presented in a further study.

CHAPTER 4

MODEL ERRORS, ANOMALY CORRELATIONS AND REPRODUCIBILITY

Root Mean Square Errors of precipitation are shown in Fig. 4.1a-d. Over South America and Africa, the largest errors are related to the overestimated precipitation, seen in the systematic errors maps (Fig. 3.2c,f,i,l), mainly in DJF and MAM. In the Indonesia region the largest errors occur in DJF and JJA. Large errors also occur to the west of Central America in all seasons, and over south of Asia in JJA.

Correlation of seasonal anomalies between the model results and the observational CMAP data set are presented in Fig. 4.2a-d. The systematic errors analyzed in the difference fields, section 3.2, showed the errors related to the precipitation values. These errors are partially removed in the correlation fields, which are related to the anomalies in each season of each year. The correlation is high over the tropical Pacific and Atlantic Oceans with very high values over eastern Pacific Ocean. This indicates that the precipitation variability in these regions is well simulated by the model. Although there are errors related to intensity or position of the Atlantic and Pacific ITCZ, the anomalies are well represented. The model response to the SST variability, which is associated to ENSO, is very good. Analyses of interannual anomaly variability have been presented in the companion paper. The correlation over Northeast Brazil is above 0.3 in all seasons. In MAM correlations of 0.5 extends to the whole Northeast. This is an important feature to rainfall prediction in this area that has the rainy season in MAM.

Other regions with high correlation are part of Indonesia region and the west equatorial coast of Africa, in JJA and SON, and areas of Indian Ocean in JJA. Positive correlations higher than 0.3 also exist in the region of the North Atlantic winter storm track. Over South America there are large areas with positive

correlation in MAM, mainly over northern, northeastern and southern Brazil. In JJA correlation higher than 0.3 is seen over southern Brazil. However, negative correlation in DJF from Amazonia to southeast indicates the inability of the model in simulating SACZ variability. In JJA there are also negative correlations over central South America and northern Argentina. In southern Africa there are positive correlations in all seasons, except in DJF when there are positive values only over southwest/west side. Large areas of positive correlation are seen over northern Africa, mainly in SON. In Australia, the highest correlations occur in MAM over the northeast and northwest, and in SON, over the northwest. Southern India has high positive correlation values in MAM and JJA, but negative values in SON. Positive correlations exist over northern and west areas of North America in DJF, and over almost the whole continent in JJA, although with lower values. Correlation values higher than 0.5 occur in areas of the North Atlantic storm track in DJF.

Reproducibility is another method of model validation, which measures the model's ability to respond consistently to the imposed boundary forcing (Sperber and Palmer 1996). It can also measure the spread of the ensemble members, as in Stern and Miyakoda (1995). Reproducibility is calculated by

$$R = \frac{\sigma^2_{\langle X \rangle}}{\overline{\sigma^2_{\langle X \rangle}}} \tag{4.1}$$

where

$$\sigma^2_{\langle X \rangle} = \overline{\left(\langle X \rangle - \overline{\langle X \rangle}\right)^2} = \frac{1}{9}\sum_{J=1}^{10}\left(\langle X_J \rangle - \overline{\langle X \rangle}\right)^2 \tag{4.2}$$

$$\overline{\sigma^2_{\langle X \rangle}} = \frac{1}{10}\sum_{J=1}^{10}\sigma^2_{\langle X_J \rangle} = \frac{1}{10}\sum_{J=1}^{10}\frac{1}{8}\sum_{m=1}^{9}\left(X_{J,m} - \langle X_J \rangle\right)^2 \tag{4.3}$$

< > is the ensemble mean , — is the time mean, j is the number of years and m is number of members.

(4.2) is a measure of the interannual variability of the signal extracted from the 9 integrations and (4.3) is the average of the variance estimates from each year based on 9 integrations. (4.2) is considered the signal, (4.3) the noise, and the reproducibility is the ratio between the signal and the noise.

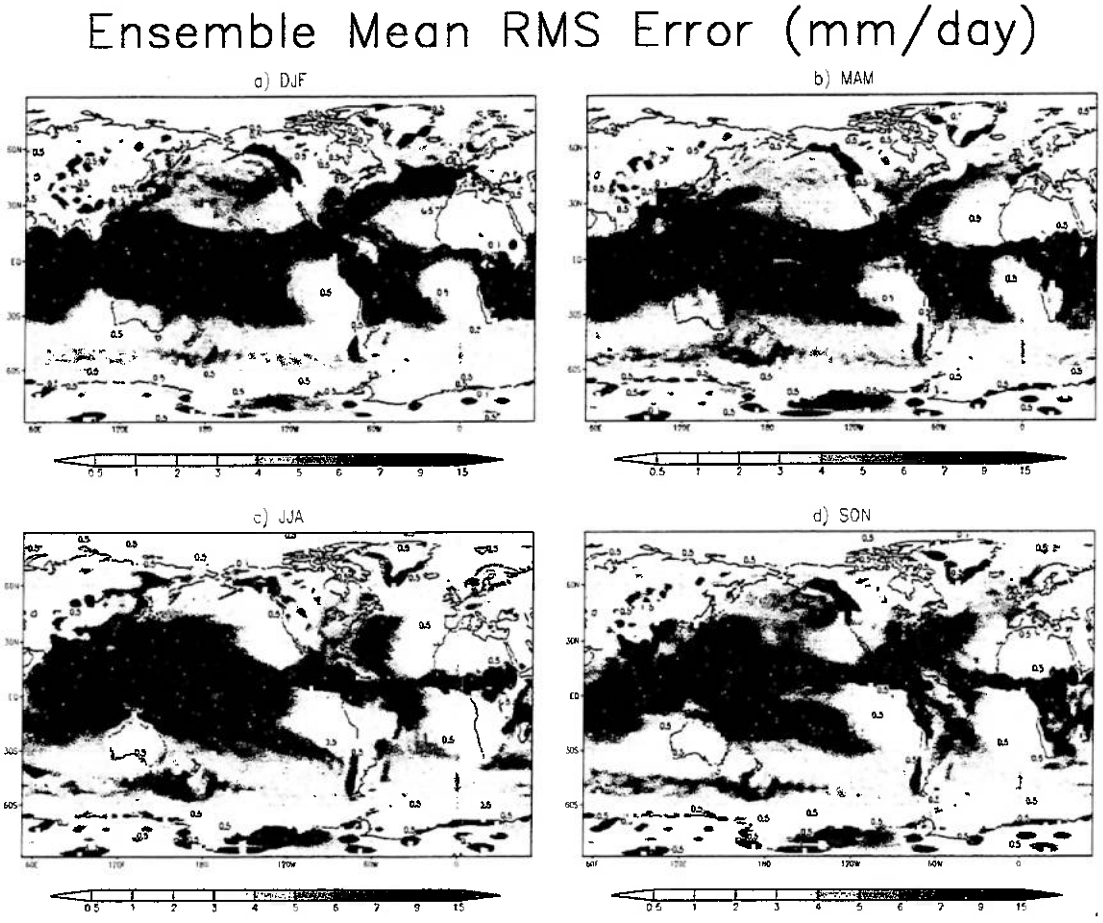

Fig. 4.1-Ensemble Mean root mean square error (a) DJF, (b) MAM, (c) JJA, (d) SON ($mm.day^{-1}$).

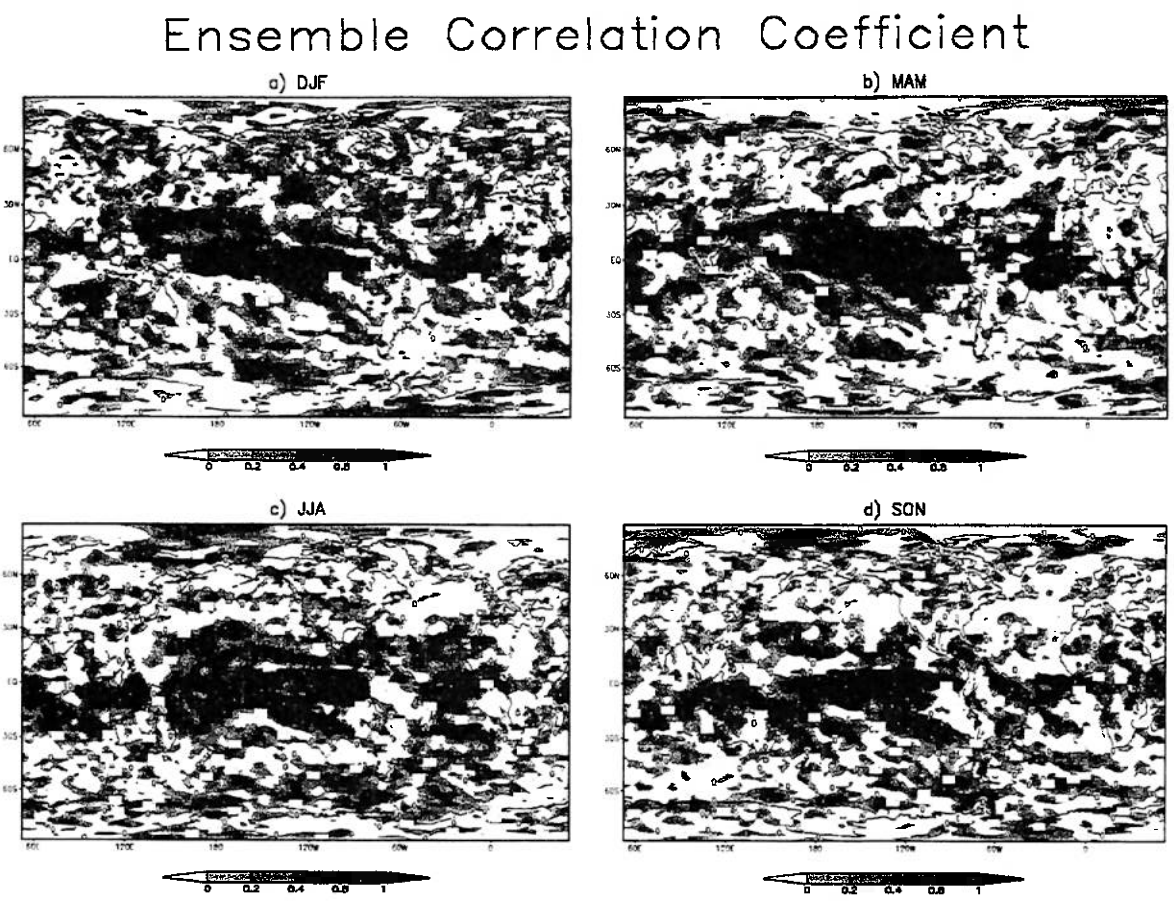

Fig. 4.2- Correlation coefficient between model anomalies and observed anomalies of precipitation, considering the ensemble mean. (a) DJF, (b) MAM, (c) JJA, (d) SON.

The largest values of reproducibility are found in the East Pacific in all seasons (Fig. 4.3). High reproducibility in this region was also found by Sperber and Palmer (1996) analysing ECMWF model results. Another similar feature to those results occurs in the Indian Ocean, where the higher reproducibility is found during northern summer (monsoon season) and in the Tropical Atlantic, where the lower reproducibility occurs in SON. Northeast Brazil and areas along the north coast of South America also show high values of reproducibility. Areas of tropical Africa and Indonesia have higher reproducibility in JJA and SON.

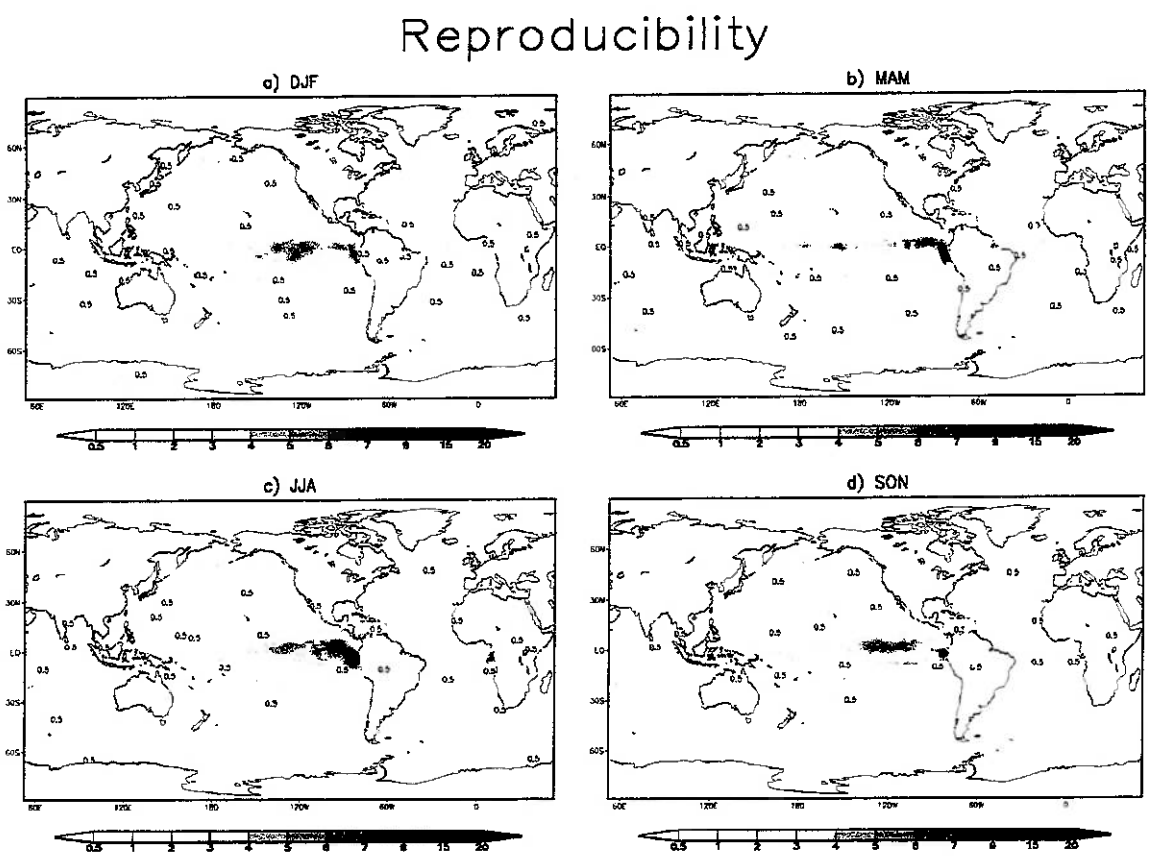

Fig. 4.3- Reproducibility (a) DJF, (b) MAM, (c) JJA, (d) SON.

CHAPTER 5

SUMMARY AND CONCLUSION

The analyses of CPTEC/COLA model climate revealed that the model is able to represent the main atmospheric features and the seasonal precipitation variability. The convection associated with the ITCZ, SPCZ and SACZ are reasonably well simulated but precipitation in the tropical sectors of the SH convergence zones is underestimated and in the extratropical sectors overestimated. There are large differences also in the Indonesia region, the oceanic areas showing underestimated values and the land island areas with overestimated values.

Large positive errors occur over northwest South America and Central America during all seasons. Negative errors tend to occur to the northwest/west of the overestimated values over South America and to the southwest/west of the overestimated values over Africa. Northern and Southern Hemisphere storm track regions are simulated in the model, however the higher than the observed values of precipitation in SH storm track may be related to higher intensity or frequency of synoptic systems. The stronger than observed jet in SH mid latitudes support this feature. Low level flow of the Indian Monsoon is well represented by the model and shows the association with seasonal precipitation variability over India/southern Asia. The direction of low level flow over the north coast of South America and the associated seasonal displacement of Atlantic ITCZ are also well simulated.

The dominance of wavenumber two in NH and wavenumber one in SH displayed by the zonal geopotential anomaly shows the ability of the model in simulating the main stationary waves of both hemispheres. The vertical structure of the dominant waves shows a large similarity with the observed structure, displaying also a wavenumber three in JJA for the South Hemisphere,

although slightly weaker in the model simulation. The meridional cell structure represents correctly the seasonal displacement of Hadley cell. The vertical structure of temperature at tropical regions and at subtropical/mid latitude regions in the SH summer are well simulated. In NH there is a negative temperature bias in summer and winter at subtropical and mid latitude regions. A strong negative temperature bias is also observed at high troposphere and stratosphere in the SH polar and high latitude regions.

Analyses of the ensemble members behaviour related to averaged precipitation over continental areas and over several areas of South America show consistency among members indicating that the ensemble mean is representative of the nine integrations. Although the root mean square errors related to precipitation values are larger in the tropical regions, the correlation coefficients are also larger in these regions, showing that the precipitation variability is better simulated there. The reproducibility fields also show that in the tropical regions the signal of seasonal variability is larger than the noise related to the spread among members.

The energy budget analyses show that there are unbalanced fluxes in the atmosphere and at the surface. The net shortwave radiative flux is larger in the model than in the observations related to the underestimation of the cloud fraction and to the neglect of the aerosol effect as well as the underestimation of the surface albedo in the model. Larger latent heat flux over the oceans in the model results imply in larger evaporation and larger precipitation rate. The imposed monthly observed SST prevent the correct interaction of fluxes between the ocean and the atmosphere, interaction that occurs between the land and the atmosphere. The COLA version of a coupled ocean-atmosphere GCM which is being implemented at CPTEC can overcome this lack of interaction, improving the energy budget. Imbalances in the energy budget were also related to the radiation scheme and cloud cover calculation, which also calls for improvements in the parameterization schemes. The deficiency of the model in simulating the amount of precipitation can be partially related to the

convection scheme. Preliminary analysis using the relaxed Arakawa-Schubert convection scheme showed overestimated precipitation over southern Amazon Region and underestimation over the northern portion. The application of another convection scheme could improve the precipitation rates, as the mass flux penetrative convection scheme (Gregory and Rowntree 1990) used by Johns et al. (1997) in the Hadley Centre coupled GCM validation.

Overall assessment of the model climate obtained from the ensemble simulation with nine members for a period of ten years reveals that the CPTEC/COLA Atmospheric GCM T62L28 version is capable of simulating all the important features of the atmosphere, thus, providing the needed validation of the model for operational weather and seasonal climate forecast guidance.

Continuous experiments and simulations are envisaged to identify errors and to improve the model response. Simulations over periods longer than ten years are necessary for statistical analyses. It is suggested the application of a different convection scheme, improvement of radiation and cloud cover scheme parametrization. Higher horizontal and vertical model resolution may also provide more accurate response in the near future.

REFERENCES

Baumgartner, A.; Reichel, E. **The world water balance: mean annual global, continental and maritime precipitation and run-off.** Amsterdan: Elsevier scientific publishers, 1975. 179 p.

Brankovic, C.; Molteni, F. Sensitivity of the ECMWF model northern winter climate to model formulation. **Climate Dynamics,** v. 13, p. 75-101, 1997.

Brankovic, C.;Palmer, T.N. Atmospheric seasonal predictability and estimates of ensemble size. **Monthly Weather Review**, v. 125, p. 859-874, 1997.

Davies, R. **Documentation of the solar radiation parameterizations in the GLAS climate model.** Washington:NASA, 1982. 57p. (NASA- Tech. Memo. 83961)

Déqué, M.; Drevelon, C.; Braun, A.; Cariolle, D. The ARPEGE/IFS atmosphere model: a contribution to the French community climate modelling. **Climate Dynamics**, v. 10, p. 249-266, 1994.

Gates, W.L. AMIP, The Atmospheric Model Intercomparison Project. **Bulletin of the American Meteorological Society**, v. 73, p. 1962-1970, 1992.

Gates, W.L. and Coauthors. An overview of the results of the Atmospheric Model Intercomparison Project (AMIP). **Bulletin of the American Meteorological Society**, v. 80, p. 29-55, 1999.

Gregory, D.; Rowntree, P.R. A mass flux convection scheme with representation of ensemble characteristics and stability dependent closure. **Monthly Weather Review**, v. 118, p. 1483-1506, 1990.

Hack, J.J.; Kiehl, J.T.; Hurrel, J.W. The hydrologic and thermodynamic

characteristics of the NCAR CCM3. **Journal of Climate**, v. 11, p. 1179-1206, 1998.

Harshvardhan; Davies, R.; Randall, D.A.; Corsett, T.G. A fast radiation parameterization for general circulation models. **Journal of Geophysical Research**, v. 92, p. 1009-1016, 1987.

Holton, J. **An introduction to Dynamic Meteorology**, Third edition, Academic Press, California, USA, 1992. 511 p.

Hou, Y.T. **Cloud-radiation dynamics interaction**. Ph.D. Thesis, Maryland, 209 pp, 1990.

Hurrel, J.W.; Hack, J.J.; Boville, B.A.; Willianson, D.L.; Kiehl, J.T. The dynamical simulation of the NCAR Community Climate Model version 3 (CCM3). **Journal of Climate**, v. 11, p.1207-1236, 1998.

Jaeger, L. (1976) Monatskarten des Niedershlags fur die ganze Erde. Ber. Dtsch. Wetterdienstes, v. 18, 38 p.

Johns, T.C.; Carnell, R.E.; Crossley, J.F.; Gregory, J.M.; Mitchell, J.B.; Senior, C.A.; Tett, S.B.; Wood. R.A. The second Hadley Centre coupled ocean-atmosphere GCM: model description, spinup and validation. **Climate Dynamics**, v. 13, p.103-134, 1997.

Kalnay, E.; Kanamitsu, M.; Kistler, R.; Collins, W.; Deaven, D.; Gandin, L.; Iredell. M.; Saha, S.; White, G.; Woolen, J.; Zhu, Y.; Leetmaa, A.; Chelliah, M.; Ebisuzaki, W.; Higgins, W.; Janowiak, J.; Mo, K.C.; Ropelewski, C.; Wang, J.; Reynolds, R.; Jenne, R.; Joseph, D. The NCEP/NCAR 40 year reanalysis project. **Bulletin of the American Meteorological Society**, v. 77, p. 437-472, 1996.

Kiehl, J.T.; Hack, J.J.; Briegleb, B.P. The simulated Earth radiation budget of the National Center for Atmospheric Research community climate model CCM2 and comparisons with the Earth Radiation Budget Experiment (ERBE). **Journal of Geophysical Research**, v. 99, p. 20815-20827, 1994.

Kiehl, J.T.; Hack, J.J.; Hurrel, J.W. The energy budget of the NCAR Community Climate Model:CCM3. **Journal of Climate**, v. 11, p. 1151-1178, 1998.

Kiehl, J.T.; Trenberth, K.E. Earths annual global mean energy budget. **Bulletin of American Meteorological Society**, v. 78, p.197-208, 1997.

Kinter III, J.L.; DeWitt, D.; Dirmeyer, P.A.; Fennessy, M.J.; Kirtman, B.P.; Marx, L.; Schneider, E.K.; Shukla, J.; Straus, D. The COLA atmosphere-biosphere general circulation model, Vol.1: Formulation. Report n^0.51, COLA, Maryland, 46 pp, 1997.

Kuo, H.L. (1974) Further studies of the parameterization of the influence of cumulus convection on large scale flow. Journal of Atmospheric Sciences, v. 31, p.1232-1240, 1974.

Lacis, A.A.; Hansen, J.E. A parameterization of the absorption of solar radiation in the earth's atmosphere. **Journal of Atmospheric Sciences**, v. 31, p. 118-133, 1974.

Lau, K.M.; Kim, J.H.; Sud, Y. Intercomparison of Hydrologic processes in AMIP GCMs. **Bulletin of the American Meteorological Society**, v. 77, p. 2209-2228, 1996.

Legates, D.R.; Willmott, C.J. Mean seasonal and spatial variability in gauge-corrected, global precipitation. **International Journal of Climatology**, v. 10, p. 111-128, 1990.

Li, Z. Ensemble atmospheric GCM simulation of climate interannual variability from 1979 to 1994. **Journal of Climate**, v. 12, p. 986-1001, 1999.

Liebman, B.; Smith, C.A. Description of a complete (interpolated)outgoing longwave rediation dataset. **Bulletin of American Meteorological Society**, v. 77, p. 1275-1277, 1996.

Marengo, J.; Druyan, L.; Hastenrath, S. Observational and modeling studies of Amazonia interannual climate variability. **Climatic Change**, v. 23, p. 267-286, 1993.

Marques, R.F.C.; Rao, V.B. A diagnosis of a long lasting blocking event over the Southeast Pacific Ocean. **Monthly Weather Review**, v. 127, p. 1761-1776, 1999.

Mason, S.J.; Goddard, L.; Graham, N.E.; Yuleva, E.; Sun, L.; Arkin, P.K. The IRI Seasonal climate prediction system and the 1997/98 El Nino event. **Bulletin of the American Meteorological Society**, v. 80, p. 1853-1874, 1999.

McFarlaine, N.A.; Boer, G.J.; Blanchet, J.P.; Laraze, M. The Canadian Climate Centre Second-Generation Circulation Model and its equilibrium Climate. **Journal of Climate**, v. 5, p. 1013-1044, 1992.

Mellor, G.L.; Yamada, T. Development of a turbulence closure model geophysical fluid problems. **Review of Geophysical Space Physics**, v. 20, p. 851-875, 1982.

Moorthi, S.; Suarez, M.J. Relaxed Arakawa-Schubert: A parameterization of moist convection for general circulation models. **Monthly Weather Review**, v. 120, p. 978-1002, 1992.

Murphy, J.M. The impact of ensemble forecasts on predictability. **Quarterly**

Journal Royal Meteorological Society, v. 114, p. 463-493, 1988.

Posey, J.W.; Clapp, P.F. Global distribution of normal surface albedo. **Geofisica International** , v. 4, p. 33-48, 1954.

Raphael, M. Quasi-stationary waves in the Southern Hemisphere: An examination of their simulation by the NCAR Climate System Model, with and without an interactive ocean. **Journal of Climate**, 11, p. 1405-1418, 1998.

Renweek, J.A. ENSO-related variability in the frequency of South Pacific blocking. **Monthly Weather Review**, v. 126, p. 3117-3123, 1998.

Reynolds, R.W.; Smith, T.M. Improved global sea surface temperature analyses using Optimum Interpolation. **Journal of Climate**, v. 7, p. 929-948, 1994.

Rowell, D. Assessing potential seasonal predictability with an ensemble of multidecadal GCM simulations. **Journal of Climate**, v. 11, p. 109-120, 1998.

Satyamurti, P.; Nobre, C.A.; Silva Dias, P.L. South America. In: Karoly, D.J.F.; Vincent D.J.F. ed., AMS. **Meteorology of the Southern Hemisphere**. Massachussets, USA, 1998, Cap.3C, p. 119-139.

Sato, N.P.; Sellers, J.; Randall, D.A.; Schneider, E.K.; Shukla, J.; Kinter III, J.L.; Hou, Y.T.; Albertazzi, E. Effects of implementing the Simple Biosphere Model in a general circulation model. **Journal of the Atmospheric Science**, v. 46, p. 2757-2782, 1989.

Slingo, J.M. The development and verification of a cloud prediction scheme for the ECMWF model. **Quarterly Journal Royal Meteorological Society**, v.13, p. 899-927, 1987.

Sperber, K.R.; Palmer, T.N. Interannual tropical rainfall variability in General

Circulation Model simulations - associated with the Atmospheric Model Intercomparison Project. **Journal of Climate**, v. 9, p. 2727-2750, 1996.

Stern, W.; Miyakoda, K. Feasibility of seasonal forecasts inferred from multiple GCM simulations. **Journal of Climate**, v. 8, p. 1071-1085, 1995.

Tiedtke, M. (1983) The sensitivity of the time mean large scale flow to cumulus convection in the ECMWF model. In: Workshop on convection in Large scale numerical models, ECMWF. **Workshop**. Reading, 1983, p. 297-316.

Wallace, J. M. The climatological mean stationary waves: observational evidence. In: Hoskins, B. and R. Pearce. **Large-scale dynamical processes in the atmosphere**. Academic Press, 1983, Cap. 3, pp.27-53.

Wang, X.L.; Zwiers, F.W. Interannual variability of precipitation in an ensemble of AMIP climate simulations conducted with the CCC GCM2. **Journal of Climate**, v. 12, p.1322-1355, 1999.

Ward, N.; Navarra, A. Pattern analysis of SST- forced variability in ensemble GCM simulations:Examples over Europe and the Tropical Pacific. **Journal of Climate**, v. 10, p. 2210-2220, 1997.

Willmott, C.J.; Rowe, C.M.; Mintz, Y. Climatology of the terrestrial seasonal water cycle. **Journal of Climatology**, v. 5, p. 589-606, 1985.

Xie, P.; Arkin, P.A. Global precipitation: A 17-year monthly analysis based on gauge observations, satellite estimates, and numerical model outputs. **Bulletin of the American Meteorological Society**, v. 78, p. 2539-2558, 1997.

Xue, Y.; Sellers, P.J.; Kinter III, J.L.; Shukla, J. A simplified biophere model for global climate studies. **Journal of Climate**, v. 4, p. 345-364, 1991.

Yang, X.Q.; Anderson, J.L.; Stern, W.F. Reproducible forced modes in an AGCM ensemble integrations and potential predictability of atmospheric seasonal variations in the extratropics. **Journal of Climate**, v. 11, p. 2942-2959, 1998.